MULTIPARAMETRIC MAGNETIC RESONANCE IMAGING OF BONE HEALING IN DOGS FOLLOWING TIBIAL PLATEAU LEVELING OSTEOTOMY

by

EMILY BURKE

(Under the Direction of Shannon Holmes)

ABSTRACT

This research primarily evaluated the efficacy of multiple different magnetic resonance imaging (MRI) sequences for monitoring of bone healing after tibial plateau leveling osteotomy (TPLO) in dogs. Titanium surgical implants were utilized intra-op in order to minimize expected susceptibility artifacts during imaging. T2-weighted DIXON, T1-weighted Turbo Spin Echo (TSE), and dynamic contrast-enhanced (DCE) sequences were used to quantify sclerosis, bone remodeling and hyperintensity and vascular perfusion at the osteotomy site 4 weeks after surgery. There was no significant correlation between MRI grades and radiographic grade of healing at 10 weeks post-operative. MRI is a feasible imaging modality for evaluation of the canine stifle after TPLO.

INDEX WORDS: MRI, bone healing, dog, TPLO

MULTIPARAMETRIC MAGNETIC RESONANCE IMAGING OF BONE HEALING IN DOGS FOLLOWING TIBIAL PLATEAU LEVELING OSTEOTOMY

by

EMILY BURKE

BS, Delaware Valley College, 2010

DVM, University of Georgia College of Veterinary Medicine, 2014

A Thesis Submitted to the Graduate Faculty of The University of Georgia in Partial Fulfillment of the Requirements for the Degree

MASTER OF SCIENCE

ATHENS, GEORGIA

2017

MULTIPARAMETRIC MAGNETIC RESONANCE IMAGING OF BONE HEALING IN DOGS FOLLOWING TIBIAL PLATEAU LEVELING OSTEOTOMY

by

EMILY BURKE

Major Professor:	Shannon Holmes
Committee:	John Peroni
	Samuel Franklin

Electronic Version Approved:

Suzanne Barbour
Dean of the Graduate School
The University of Georgia
May 2017

ACKNOWLEDGEMENTS

I would like to acknowledge each of my committee members for their support, criticisms, and unwavering dedication to my pursuit of this degree. Additionally, this project could not have been completed without the inspiring assistance of the veterinary technicians in both the department of research as well as in the Veterinary Teaching Hospital. I am grateful to and for each and every one.

TABLE OF CONTENTS

Page

LIST OF TABLES

Page

LIST OF FIGURES

Page

CHAPTER 1

INTRODUCTION AND LITERATURE REVIEW

Introduction

Rupture of the cranial cruciate ligament is the leading cause of lameness in dogs in the United States, with an estimated 1.2 million surgeries performed each year for treatment[1]. Owner preference and patient size largely dictates the treatment methods pursued, but tibial plateau leveling osteotomy (TPLO) is the procedure most commonly employed by veterinary surgeons to treat cranial cruciate ligament rupture. Radiography is most routinely utilized for monitoring these patients post-operatively [2], primarily because it is readily available in private practice and economically affordable for most pet owners. Despite its utility, radiography does not provide information about osseous vascularity or changes within the metaphysis that occur during healing, and the presence of metallic implants can prevent complete evaluation of all osseous margins.

Magnetic resonance imaging is a commonly utilized form of diagnostic imaging for human patients [3]. It is considered a noninvasive method of evaluation of musculoskeletal disease, though the need for general anesthesia to facilitate MRI in veterinary patients means that it is not a completely benign procedure. It is superior to radiography in its contrast resolution, in that it can more readily identify differences between tissue types [4]. Vascular conspicuity, subtle changes within bone indicative of inflammation or infection, and superior soft tissue resolution all contribute to its utility for patients post-operatively. Though it is routinely used for diagnosis and monitoring of neurologic disease in the veterinary patient, musculoskeletal imaging is

relatively new. Previous work has used primarily low-field magnets, and there has been no work done investigating the effects of titanium bone plates on imaging in veterinary patients.

The purpose of this research was to describe the utility of multiparametric magnetic resonance imaging for monitoring of bone healing after performance of TPLO in dogs. Information garnered from the study could be used in the future to identify causes for and predict delayed or incomplete osseous healing in the canine patient.

Magnetic Resonance Imaging – Basic Physics

Magnetic resonance imaging, or MRI, utilizes the inherent magnetic identity of atoms within tissues to generate an image [5]. Utilized routinely for musculoskeletal imaging in human medicine, it has been gaining popularity within the veterinary field for its utility in the diagnosis of both neurologic and musculoskeletal disease processes. An introduction into its physics is required to better understand how MRI can detect both anatomical and physiologic alterations, where most diagnostic imaging modalities are more limited to anatomical alterations

The magnetic identity of an atom is characterized by several factors, including mass number, atomic spin and overall atomic charge [6]. The mass number is the sum of the neutrons and protons within its nucleus, which dictates its net charge and consequently determines whether or not it will spin and ultimately resonate. A nucleus that has an odd mass number, in which the number of neutrons does not equal the number of protons, will spin on its own. This is in contrast to a nucleus with an even mass number, where the individual spins will cancel each other out and result in the absence of a spin[7]. The spinning of odd mass numbered nuclei is random, and the moving, unbalanced charge will create a magnetic field with a unique direction and size. The term "magnetic moment" is used to describe the direction and size of each nuclear magnetic field.

Only nuclei possessing a magnetic field are considered to be magnetic resonance (MR) active. Some MR active nuclei include fluorine, phosphorous, sodium, oxygen and hydrogen[8]. The hydrogen atom is the MR active element most commonly utilized for MRI [6 9 10 4]. One of the primary reasons is its concentration within the mammalian body, especially within fat and water. It exists at substantially higher concentrations than the other isotopes and as a result of this higher concentration, images with diagnostic resolution and quality are formed in a shorter period of time than if the other isotopes were used[7].

In the presence of an external magnetic field, the hydrogen atom will additionally wobble, or precess, at a specific frequency referred to as the Larmor frequency[7]. The strength of the magnetic field dictates the Larmor frequency: increasing field strength will increase the Larmor frequency [11]. Hydrogen atoms are capable of only two energy states and thus their magnetic moments can only align parallel or antiparallel to this external magnetic field, with slightly more aligning in the parallel direction [9]. At any given time point one magnetic moment can be cancelled out by another magnetic moment in an opposing orientation [11]. The hydrogen atoms within a particular tissue can additionally be described as either out of phase or in phase [6]. Out of phase describes differing locations of each magnetic moment along its own precessional path. In phase means that each magnetic moment is at the same location as the surrounding or nearby magnetic moments. Phase direction is one variable that can be manipulated during magnetic resonance imaging.

Resonance occurs when one object vibrates at the same natural frequency as a second nearby object, and consequently induces the second object into vibrational motion [5]. It is considered a transfer of energy, or an energy transition. In MRI, the application of a radiofrequency (RF) pulse at the Larmor frequency provides the energy to change the existing

energy state of the precessing nuclei. Each precessing hydrogen atom has a net magnetic direction which is denoted as the net magnetization vector (NMV) [11]. The NMV, representative of the balance between parallel and antiparallel alignments, will change angulation between the longitudinal and transverse planes of tissue depending on the intensity of the RF pulse. This angulation is referred to as the flip angle [12]. As an example, if the RF pulse is directed 90° to the external magnetic field, it will induce a 90° flip angle of the NMV.

External manipulation of magnetic field strength is done through specifically located coils of wire, referred to as gradients, which exist within the bore of the MRI unit. There are three sets of gradients organized in the Cartesian planes, identified as the X, Y and Z gradients [11]. Imposition of a gradient-based magnetic field can change the field strength in linear fashion from -1 to +1. These small alterations produce small changes in the precessional frequency and phase of the nuclei to spatially encode the different spinning nuclei. The exact center of the intersecting three gradients is referred to as the isocenter, and is the optimal location of anatomy of interest when conducting a scan [13]. Slice location selection as well as frequency and phase encoding directives are applied by the operator utilizing these gradients in order to obtain desired images[6].

Frequency encoding refers to the ability to spatially locate a signal along the long axis of an image [14]. The long axis gradient identifies this signal by locating areas which have experienced a change or shift in frequency after protons are exposed to RF pulses. This type of encoding is turned on specifically during the echo period. Phase encoding similarly provides information about the spatial location of signals [14]. Instead of obtaining signal from areas based on changes in frequency, this gradient identifies areas in which a phase shift has occurred. Both phase encoding and frequency encoding gradients can be manipulated by the operator and are the

most common source of image artifacts [15], such as motion or chemical shift. Each of those artifacts have important implications in veterinary musculoskeletal MR imaging.

Slice selection is performed for each of the three gradients, with the Z gradient corresponding with axial slices, the Y gradient corresponding to the dorsal/coronal slices and the X gradient corresponding to the sagittal slices [6]. Each slice will be excited individually after application of an RF pulse with a specific bandwidth or range of frequencies. The thickness of each slice is determined by the operator. Thinner slices generally provide an improved spatial resolution, but contain fewer protons and therefore generally yield less signal for detection[16]. Another manipulation related to slice selection is insertion of a gap or skip between consecutive slices. The purpose of these gaps is to prevent cross-talk artifact, with the added benefit of decreasing overall scan time [17].

Coils are specialized instruments utilized in MR imaging to both transmit RF pulses and receive the resulting signal. The three main types of RF coils are: transmit/receive coils, surface coils, and phased array coils [6]. Each coil is largely defined by the role it plays in MR imaging, and the number of transmit and/or receive elements within it [18]. A transmit/receive coil will both transmit the RF pulse and then also receive the MR signal. After stimulation with an RF pulse to induce resonance, the NMV's of hydrogen nuclei will cross over the path of the coil. When they do, they induce a specific voltage within the coil. This voltage is recorded and used to produce an image [18]. For the purposes of our study, a 15-channel transmit/receive knee coil (TxRx Knee 15, Siemens, Erlangen, Germany) was utilized, organized as 3 rows of 5 elements. This type of coil is used frequently in human musculoskeletal imaging due to its improvements in image homogeneity[19]. It is made to completely surround the area of interest, similar to other purpose-design coils such as those for head and neck, breast, and smaller appendicular imaging.

Application of a 90-degree RF pulse flips the NMV of excited protons 90 degrees into the transverse plane. Removal of this pulse allows their magnetization to return to the longitudinal direction, with different tissues relaxing at different rates. This process is referred to as T1 relaxation, or spin-lattice relaxation. The *lattice* is the molecular structure and arrangement of the hydrogens within the tissue[13]. As the magnetization relaxes, the energy created by excitation is released back into this lattice. By definition, T1 represents the time it takes for the longitudinal magnetization to reach 63% of its total value. Images that are T1-weighted(w) have contrast due to differences in the T1 relaxation times between tissues. Production of a T1w image requires manipulation of the repetition time (TR) and time to echo (TE), both of which are controlled by the MR operator. The TR represents the amount of time that passes between successive 90-degree RF pulses, and the TE is the amount of time that passes between the application of a RF pulse and acquisition of the signal that's generated. Generally a T1w image, the TR will be between 300-600 ms and TE between 3-30ms [6,20]. On T1w images, tissues with short relaxation times (e.g. fat) will be bright and those with long relaxation times will be dark (e.g. water).

The initial 90-degree RF pulse causes phase coherence of the protons. After removal of the RF pulse, this phase coherence is lost due to inhomogeneities between different tissues {Bushberg:vq}. T2 relaxation, also referred to as free induction decay or spin-spin relaxation, represents the time it takes for transverse magnetization signal to decay to 37% of its original value[6]. As opposed to spin-lattice relaxation, in spin-spin relaxation energy is exchanged between protons without the energy being lost [21]. Similar to T1 contrast, contrast in T2w images is due to differences in tissue composition yielding differing rates of decay. This contrast is achieved by manipulation of the TR and TE parameters: the TE should be long enough that both fat- and water-composed tissues have had time to decay, and a longer TR is employed to

diminish T1 effects. Generally for a T2w image, a TR of >3000 ms and TE of >70 ms are used {Bushberg:vq} [6]. Those tissues which decay quickly (e.g. tendon) will be appear dark, and those which take longer to decay (e.g. water) will appear bright on the final images produced.

The third method of interrogating the resonating protons is to simply consider the number of protons within a tissue, or a so-called proton-density (PD)-weighted image. In this type of imaging, contrast is achieved by measuring the difference in the number of magnetized protons within a volume of tissue [20]. This method is considered a type of intermediate weighting because it utilizes some aspects of both T1 and T2. T1 effects are diminished through use of a long TR (>2000 ms), and T2 effects are diminished through use of a short TE (generally 10-30 ms) [6]. Those tissues with a high concentration of protons will appear bright on resulting images. Inversely, tissues with a low concentration of protons will appear dark. Regardless of weighting, some substances will always appear dark in MRI. This is because their protons are tightly bound and, as a result, cannot resonate. The most common examples of these types of material include air and cortical bone.

Signal acquisition is relatively straightforward in concept, but can be affected negatively by multiple factors. Some undesired signal, referred to as noise, is always present during an MR study and in the resultant image. This noise can come from the patient, the environment surrounding the patient, or the MR system itself. During image acquisition we monitor the ratio of desired to undesired signal (the signal to noise ratio, or SNR) with the need to maintain it above a certain value in order to create diagnostic images. This value can vary between machines, as SNR is affected by magnetic field strength and type of RF coil used among other things. The goal is to optimize SNR without increasing overall scan time to impractical lengths for clinical imaging.

Another factor that affects signal acquisition is artifact production. When imaging live patients, respiration and pulsatile vascular motion can cause image blurring or repeating artifacts in the phase encoding direction. Since most clinical veterinary studies are performed with our patients under general anesthesia, gross movement artifacts are limited. One commonly encountered artifact when imaging veterinary patients is that caused by metal implants such as microchips and orthopedic implants from prior surgeries. The composition of these objects typically has a ferromagnetic component, which dictates a high magnetic susceptibility in the face of an external magnetic field[22,23]. The difference in magnetic susceptibility of these implants and adjacent tissues leads to local magnetic field inhomogeneities and is the source of artifact[24]. The resulting artifact can manifest as geometric distortions in signal, signal loss or void and signal accumulation also known as signal pile-up in the frequency encoding direction. Depending on the location of the implant, these types of artifacts can profoundly affect the image quality and mask pathologic change.

There are times in which we utilize the magnetic susceptibility of particular substances to our advantage during MRI. One example is in the administration of contrast media during an MR study. The most commonly utilized contrast agent is gadolinium (Gd), a paramagnetic substance with a large magnetic moment due to its 7 unpaired electrons. An unpaired electron has a magnetic moment that is 657 times that of a proton (Wolbarst book 2013), and when in close proximity to hydrogen atoms this increases their rate of energy transfer. The transfer of energy from a nucleus to its surrounding environment is the hallmark of T1 recovery, therefore Gd shortens T1 relaxation time and is considered a T1 enhancing agent. Contrast agents such as Gd are used clinically to highlight inflammation, identify and characterize tumors, and identify vessel patency and morphology.

Understanding the basic physics behind MRI is vital to the development of imaging protocols. This study presented an opportunity to develop an MRI protocol for sequence optimization in the face of metal implants, as well as to investigate the utility of pre- and post-contrast imaging to identify changes associated with osseous healing and vascularity after performance of tibial plateau leveling osteotomy in dogs. A review of the literature associated with metal artifact reduction and sequence selection for musculoskeletal magnetic resonance imaging is discussed in successive chapters.

Post-Operative MR Imaging: Overcoming Metal Artifact

Particularly when general anesthesia is not required, MRI represents a non-invasive means for identifying post-operative complications that cannot be appreciated with other diagnostic imaging modalities. In human medicine, elective surgeries which involve metallic implants such as spinal fusions and total hip and total knee arthroplasties are increasingly performed, and despite appropriate pre-operative and surgical techniques, complications do arise. As an example, in 2007, 300,000 spinal fusions were performed in the United States with complication rates as high as 30-40%[25]. Early diagnosis of these complications is crucial for appropriate post-operative management, and the superior soft tissue contrast provided by MRI has propelled it forward as the modality of choice for neurologic and musculoskeletal imaging in human medicine[26].

Any medical implant that is licensed for use in human medicine must undergo testing to ensure it is safe within the MR environment. In particular, evaluation for the likelihood of implant migration due to the external magnetic field as well as for the possibility of implant heating are performed. In veterinary medicine, the most commonly encountered source of metal artifact are the radiofrequency identification devices, or microchips, located subcutaneously

between the shoulder blades of almost every canine patient[27]. Due to an increase in the number of patients with microchips, studies have been performed to evaluate for implant heating and migration during MRI[22,28]. Both studies showed no significant implant heating nor any associated pathologic changes to the tissues immediately surrounding the devices. Additionally, there was no change in position of the microchip compared to its location before MRI.

The common subcutaneous location between the shoulder blades in veterinary patients means the artifact caused by microchips is often encountered when performing MR exams of the cervicothoracic spine. This susceptibility artifact is characterized by significant signal loss and general image distortion over a large area of tissue surrounding the microchips. Though previously mentioned studies illustrated that the chips do not directly affect patient safety, significant signal loss and image distortion can interfere with diagnosis and therefore affect the general wellbeing of the patient[27]. For smaller patients in which the chip lies within 2-3cm of the spinal cord, there is the potential for complete image obliteration of tissue of interest due to this artifact[28].

Though many implants utilized in human medicine contain titanium alloy elements, it remains an uncommonly employed metal for our veterinary patients: most plates, pins, wires, and screws, and all microchips, are made of stainless steel or other ferromagnetic substances. One common exception is the titanium allow implants used for tibial tuberosity advancements (TTA), another procedure performed for management of cranial cruciate ligament rupture. A recent study in dogs described the effect of surgical implants on the ability to discern articular and periarticular stifle anatomy using MRI after receipt of TPLO, TTA or extracapsular stabilization for treatment of cranial cruciate ligament rupture[23]. They concluded that implants composed of titanium alloy (e.g. those used for TTA) produced much less artifact and allowed

for satisfactory evaluation of intra- and periarticular anatomy. This result is largely because titanium is non-ferromagnetic and so inherently has a smaller magnetic susceptibility, therefore creates smaller susceptibility artifacts. In our study, the primary area of interest (the osteotomy site) would lay immediately adjacent to and within 3 cm of the medially-applied TPLO plate. In order to reduce susceptibility artifacts and image obliteration of tissue of interest during our MR exams, we chose to use custom titanium plates and screws.

Though they are non-ferromagnetic, there is still a large difference in magnetic susceptibility between titanium implants and adjacent tissues and so artifact is still present[29]. Mentioned previously, the observed susceptibility artifact is characterized by signal void, signal pile-up, and geometric distortion of the implant margins and adjacent anatomy. The field inhomogeneity caused by differences in magnetic susceptibility result in more rapid dephasing of protons after an RF pulse, which results in overall signal void. These variations in the magnetic field similarly result in frequency inconsistencies, which lead to a displacement and artificial accumulation of signal in one region (pile-up). The less extreme versions of artifact caused by frequency variations are represented as geometric image distortion [25].

A technique commonly employed for management of susceptibility artifact involves increasing the bandwidth (BW) for each sequence. The BW represents the amount of frequencies which can be transmitted and/or received within a limited amount of time. The receiver BW can be manipulated in a sequence by the operator. More specifically, increasing the receiver bandwidth leads to a decrease in echo time, which decreases the severity of artifacts[30]. One description for optimization of sequence parameters included a minimal anecdotal receiver bandwidth of greater than 500 Hz/pixel being necessary for adequate artifact reduction[16]. While increasing the receiver bandwidth can reduce metal artifacts at higher field strengths, there is a

maximum limit in place for each machine. These limits are directly related to both patient safety as well as overall cost of appropriate MR hardware[31].

In addition to increasing receiver bandwidth, view angle tilting (VAT) can be utilized to manage metal artifact. VAT works by applying an additional gradient in the slice-encoding direction when signal is being read. This gradient tilts the signal being sampled and compensates for the frequency shifts caused by field inhomogeneities[16]. Its specific purpose is to correct for in-plane signal displacements, but application of VAT can negatively affect image quality by increasing image blurring[32]. This blurring can be reduced through implementation of a large receive bandwidth.

Another method for reduction of susceptibility artifacts is the use of shorter echo times (TE) in MR studies. By decreasing the amount of time between application of an RF pulse and collection of signal, we are able to avoid premature loss of signal due to magnetic susceptibilities[16,23,25]. As the echo time is directly related to whether an image is T1- or T2-weighted, there are limitations to how much it can be decreased depending on weighting goals. Repeated echoes within a single acquisition are similarly beneficial and the basis of the turbo spin-echo (TSE) pulse sequence. In this sequence, multiple 180° rephasing pulses are applied, each creating their own spin echo for reading. The combined data from each echo is used to form the final image. Though inherently each echo will have its own TE, the effective TE which is controlled by the unit operator will dictate the final image appearance. The MR system will order phase encodings in a way that those which produce the most signal will be those closest to the effective TE[6]. The greater the number or echoes, or echo train length, the better the artifact reduction.

Two sequences have been developed specifically for management of susceptibility artifacts associated with metallic surgical implants. One such sequence is referred to as SEMAC, or slice-encoding metal artifact correction. Developed by and for Siemens MR units, it applies an additional slice-encoding gradient onto a standard fast-spin echo sequence. The other was developed for General Electric MR units and is called MAVRIC, standing for multiacquisition variable-resonance image combination. MAVRIC is a 3-dimensional sequence which uses multiple and overlapping volumes of tissue at different frequency offsets to minimize artifact. Our institution employs a high-field (3T) Siemens Magnetom Skyra MRI unit, and so SEMAC parameters were available for our use. One additional option is the WARP-TSE sequence. This combines view angle tilting, SEMAC, and an increased bandwidth in order to mitigate susceptibility artifacts[33].

In order to maximize reduction of susceptibility artifacts in MR imaging, utilization of TSE pulse sequences with increased BW, VAT, and techniques for reduction of through-plane artifacts should be employed. Additionally, the use of nonferromagnetic surgical implants, such as those made with titanium alloy, can further reduce the severity of artifact. Those factors were all considered and employed in the development of MRI protocols for this study.

MRI Pulse Sequence Selection for Evaluation of Bone Healing

Each individual MR parameter, e.g. time to echo, repetition time, BW, etc., can be manipulated by the operator and assembled into a pulse sequence protocol to completely define pathologic changes of disease. These sequences are named generally for their weighting, the plane of tissue being imaged, and for any unique parameter changes. In radiography, images must be acquired in a minimum of 2 orthogonal planes in order to provide appropriate spatial orientation. The superior contrast resolution of MRI allows for maximal evaluation of certain and

differing anatomical structures within different planes. This negates the need for orthogonal planar imaging in order to identify abnormalities based on spatial resolution. In musculoskeletal MR imaging of the veterinary patient, acquisition of sagittal, dorsal and transverse plane images is performed in reference to specific anatomy. As in human musculoskeletal imaging, the most commonly utilized pulse sequences are two-dimensional fast-spin echo sequences for specific contrast and resolution. Employment of three-dimensional sequences allows for reconstruction of the acquired images into any other or oblique planes. An added benefit for three-dimensional imaging is decreased overall scan time, as one sequence can potentially take the place of three[19].

Musculoskeletal MR imaging protocols typically contain a minimum of three sequences: a T1-weighted sequence, a T2-weighted sequence, and an intermediate-weighted sequence, all of which can be acquired with or without fat saturation[34]. Each sequence provides information about different types of tissues, and final image interpretation relies on the combined evaluation of sequences. Related to musculoskeletal imaging, T1-weighted sequences highlight fat (high or bright signal) and sclerosis (low or dark signal). T2-weighted sequences highlight synovial fluid, edema and related inflammation (high or bright signal). Some tissues, such as cortical bone, will have no signal no matter the weighting of the sequence. Our study involved MR imaging of the canine stifle 4 weeks after performance of TPLO. For evaluation of osseous healing, we were primarily interested in the degree of sclerosis, evidence of bone hyperintensity and/or edema, and general vascularity of the osteotomy site and surrounding tissues.

The TPLO involves creation of a curvilinear osteotomy, or cut through the bone, within the proximal aspect of the tibia. Though intentional, the osteotomy line represents a fracture through both cortices and the medullary cavity. Especially for those fractures which are nondisplaced, the utility of MRI over radiography for diagnosis is unmatched. Fracture lines can

have variable signal in MR imaging, based on both the stage of disease as well as the type of fracture[35,36]. Though timelines for radiographic signs of osseous healing are widely accepted, the development of similar timelines using MRI are still in process.

There are multiple physiological processes that occur during normal fracture healing, generally grouped into three overlapping phases: acute inflammation and hemorrhage, callus formation, and osseous remodeling[37]. The inflammatory phase is short-lived and a soft connective tissue callus is formed at the fracture site by 2-3 weeks after injury. By 4-weeks post-op the soft callus is increasingly sclerotic as fibrous tissue and cartilage fills the fracture gap. The degree of sclerosis can readily be determined using a T1-weighted MR sequence and utilized to identify patients in which osseous healing is progressing as expected[36]. Sclerosis is characterized by hypointense or dark signals radiating away from the fracture line. It can be analyzed quantitatively through measurement of pixel intensities, with lower mean values within a region of interest representing increased sclerosis. One recent paper evaluating fracture dating in human medicine demonstrated a decline in values for T1w pixel intensities over time[36]. They suggested that this decline was due to an increase in the concentration of paramagnetic substances during fracture healing, such as methemoglobin. Additionally, they demonstrated a strong variation in values for both T1- and T2-weighted sequences during the early phases of fracture healing likely due to variation in stages of healing for each patient.

Additional markers of osseous injury and healing include the presence of bone edema and inflammation. Both processes are identified on MR imaging with the same high (or bright) signal as fat. In order to differentiate between edema/inflammation and fat, the signal from fat must be suppressed. There are multiple techniques for achieving fat suppression, though the Dixon technique is preferred in human musculoskeletal imaging as it provides the best homogenous fat

suppression without signal loss[38-40]. Dixon first proposed a two-point MR imaging technique in 1984 which utilized acquisition of 2 separate images, one in which the fat and water molecules of tissue were in phase with each other and another in which they were at 180° out of phase. Post-acquisition subtraction techniques could then be applied in order to acquire "pure water" images with fat suppression and "pure fat" images with water suppression[41]. Compared to other techniques, the shorter acquisition time without loss of SNR propelled the popularity of this method of fat suppression, particularly in pediatric or elderly patients. More recently the Dixon technique has been tested against other methods of fat suppression and proven to provide more effective suppression independent of imaging plane selected[42].

Crucial to normal osseous healing is the establishment of appropriate vascular perfusion at the fracture site. Poor or absent perfusion has been associated with abnormal or even incomplete osseous healing[43]. In human medicine, fracture non-unions, or a failure to heal, have reported rates of 5-15% depending on fracture location, the degree of soft tissue damage and site contamination[44]. Though similar rates in veterinary medicine are unreported[45], anecdotal descriptions of their prevalence exists, as well as the propensity for affected patients to experience catastrophic complications as a result. In MR imaging of the musculoskeletal system, dynamic contrast-enhanced (DCE) sequences have been extensively evaluated for their ability to predict those patients more at-risk for developing fracture non-unions.

DCE involves acquisition of multiple consecutive T1w images after administration of an intravenous paramagnetic contrast solution. T1w is used so that rapid changes in signal intensity during the arterial and venous flushes of contrast enhancement can be evaluated[46]. Each acquisition occurs over a set period of time (e.g. every 10 seconds) with upwards of 25 consecutive acquisitions typically made. The resulting images are then analyzed for change in

signal intensity in a particular region of interest, such as a fracture site. They can then be used to identify and quantify absent, poor, and/or adequate osseous perfusion.

During the early phase of fracture healing there is a 20 times greater vascular supply within a fracture site compared to resting circulation, which persists for 3-10 weeks after injury[47]. Multiple studies in human medicine have been performed to establish values for sensitive identification of nonunion fractures as well as for the presence of infection[44,47-49]. These studies additionally identified variations in vascular enhancement patterns that correlated with the benign or malignant nature of areas of interest imaged. This technology is available but underutilized in veterinary musculoskeletal imaging, primarily due to both the requirement for general anesthesia as well as operator comfort with dynamic image acquisition.

In summary, MRI is an effective and non-invasive imaging modality for the monitoring of osseous healing. Specific pulse sequences are selected for use in musculoskeletal imaging for their ability to efficiently identify areas of fracture, sclerosis, edema/inflammation, as well as perfusion. As pulse sequence technologies and methodologies become available in human medicine, their applications for the veterinary patient warrant investigation.

CHAPTER 2

THE EFFECT OF PLATELET-RICH PLASMA ON OSSEOUS HEALING IN DOGS UNDERGOING HIGH TIBIAL OSTEOTOMY[1]

[1] Samuel P. Franklin, Emily E. Burke, Shannon P. Holmes. Submitted to *PLOS ONE,* 01/29/17

ABSTRACT

Objectives

The purpose of this study was to investigate whether platelet-rich plasma (PRP) enhances osseous healing in conjunction with a high tibial osteotomy using a canine model.

Study Design

Randomized controlled trial

Methods

Sixty-four client-owned pet dogs with naturally occurring rupture of the anterior cruciate ligament and that were to be treated with a high tibial osteotomy (tibial plateau leveling osteotomy) were randomized into the treatment or control group. Dogs in the treatment group had autologous platelet-rich plasma activated with calcium chloride and bovine thrombin to produce a well-formed PRP gel that was placed into the osteotomy at the time of surgery. Dogs in the control group had saline lavage of the osteotomy. All dogs had the osteotomy stabilized with identical titanium alloy implants and all aspects of the surgical procedure and post-operative care were identical among dogs of the two groups. Bone healing was assessed at exactly 28, 49, and 70 days after surgery using radiography and ultrasonography and using MRI at day 28. The effect of PRP on bone healing was assessed using a repeated measures analysis of covariance with radiographic and ultrasonographic data and using a t-test with the MRI data.

Results

Sixty dogs completed the study. There were no significant differences in age, weight, or gender distribution between the treatment and control groups. Twenty-seven dogs were treated with PRP and 33 were in the control group. The average platelet concentration of the PRP was

$1.37x10^6$ platelets/µL (±$489x10^3$) with a leukocyte concentration of $5.45x10^3$/µL (±$3.5x10^3$). All dogs demonstrated progressive healing over time and achieved clinically successful outcomes. Time since surgery and patient age were significant predictors of radiographic healing and time since surgery was a significant predictor of ultrasonographic assessment of healing. There was no significant effect of PRP treatment as assessed radiographically, ultrasonographically, or with MRI.

Conclusion

The PRP used in this study did not hasten osseous union in dogs treated with a high tibial osteotomy.

INTRODUCTION

Improving the rate and effectiveness of osseous healing after fracture, bone loss, or osteotomy remains a clinically relevant goal in orthopedic research[50,51] Anabolic growth factors such as transforming growth factor betas, vascular endothelial growth factor, and platelet-derived growth factors are contained in abundance within platelet alpha granules and their delivery to fracture or osteotomy sites could theoretically stimulate osseous regeneration[52] As a result, platelet-rich plasma (PRP) has commonly been investigated for its role in augmenting bone regeneration in both preclinical models and clinical studies in people. Multiple reviews have been performed of the available data[53-56]. Many data from pre-clinical models provide support for the benefits of PRP in augmenting osseous union and some authors conclude there is sufficient evidence to demonstrate proof of principle[56]. However, other authors conclude that the evidence remains ambiguous as numerous studies, particularly when considering clinical trials in people, fail to provide consistent or convincing evidence of benefit[55]. Contradictory results from different

studies and contradictory conclusions from different reviews preclude making a general conclusion as to whether PRP is likely to augment bone healing.

Some of the possible reasons for discrepant results include investigation in different species, use of PRP with different bone defect or fracture models, use of different PRP products, and use of different outcome measures to assess efficacy. All of these variable have likely contributed to the extreme heterogeneity in the data available[55]. As a result, further research is needed to determine which specific types of PRP may be beneficial in improving bone healing and in which specific medical conditions. In order to address this issue there is a need for well-controlled experiments using thoroughly characterized PRP products, including in preclinical animal models.

Treatment of anterior cruciate ligament (ACL) rupture in client-owned pet dogs provides a potentially useful and unique model for assessing the effects of PRP on bone healing. Naturally-occurring rupture of the (ACL) is extremely common with one report estimating that 1.2 million surgeries are performed each year in the USA to treat ACL rupture in dogs[1]. High tibial osteotomy, and more specifically tibial plateau leveling osteotomy (TPLO), is one of the most commonly performed surgeries to treat dogs with ACL rupture[57]. This surgery involves performing a cylindrical osteotomy of the proximal tibia and de-rotating the proximal tibial to decrease the tibial plateau angle (posterior tibial slope), thus minimizing femorotibial subluxation and helping them cope with being ACL-deficient (Figures 2.2 and 2.3)[58]. Although results with this procedure are usually good, complications can include delayed osseous union, nonunion, and mechanical failure with loss of reduction prior to attainment of osseous union[59,60]. Accordingly, if a PRP were effective in enhancing the rate of osseous union it would have clinical utility for dogs treated with TPLO. In addition, should a PRP augment bone healing in

dogs treated with TPLO, a human PRP with similar characteristics would be worthy of investigation for its potential application in people.

The purpose of this study was to investigate the utility of a well-characterized PRP for enhancing osseous union in dogs treated with TPLO and using multiple clinically-applicable outcome measures including radiography, ultrasonography, and magnetic resonance imaging (MRI). We hypothesized that dogs treated with PRP would have more rapid healing of their osteotomy as assessed with radiography and MRI than dogs not treated with PRP. Further, we hypothesized that MRI would prove more sensitive than radiography or ultrasonography for assessing early healing of the trabecular bone of the proximal tibial metaphysis.

METHODS

Study subjects

Sixty-four client-owned pet dogs with naturally-occurring rupture of the ACL were enrolled in this prospective, randomized, blinded clinical trial. This study was approved by the Clinical Research Committee at the University of Georgia. Enrollment criteria included that the dog needed to be diagnosed as having ACL rupture based upon orthopedic examination and pre-operative radiography as is routinely performed for dogs with ACL rupture. Further, all dogs were between 2 and 10 years of age and weighed at least 25 kilograms. All dogs needed to have a tibia that was of appropriate size to be treated with a 21 mm radius TPLO saw blade and stabilized with a 6-hole custom TPLO plate. All dogs were free of any other medical problems and were not receiving any medications at the time of TPLO.

Enrolled dogs were randomly assigned to either the treatment (PRP) or control (saline) group using a random number generator. All dogs were anesthetized using the same anesthetic medication protocol including pre-medication with 0.005 mg/kg body weight of

dexmedetomidine (Zoetis, Florham Park, NJ) and 0.1 mg/kg of hydromorphone (Hospira Inc, Lake Forest, IL). Anesthesia was induced with 5 mg/kg of Ketamine (Akorn, Lake Forest, IL) and 0.25 mg/kg of diazepam (Hospira, Lake Forest, IL) and maintained with Isoflurane (Piramal, Bethlehem, PA).

Once anesthetized, and immediately preceding surgery, an 18-gauge 2-inch intravenous catheter was aseptically placed in a jugular vein for those dogs included in the PRP group. Fifty-two mls of blood was collected into two 60-ml syringes preloaded with 8mls of ACD-A to provide a total volume of 120 ml of anticoagulated blood. A 0.5 ml aliquot of this blood was mixed with ethylenediaminetetraacetic acid (EDTA) and then assessed to characterize the cellular concentrations in the whole blood using an automated hemacytometer (Element HT5, Heska Corporation, Loveland, CO). The sample was mixed with EDTA prior to assessment of the cellular composition as some evidence suggests that use of EDTA prior to analysis optimizes platelet enumeration[61]. The remaining anticoagulated blood was used to prepare PRP using a commercially available system (Angel System, Arthrex Vet Systems; Naples, FL). After preparation, an aliquot of the PRP was similarly mixed with EDTA and assessed using the same hemacytometer similar to previous work[61].

After blood acquisition and while the PRP was being prepared, surgery was commenced including arthroscopic evaluation of the affected stifle and intra-articular structures including the ACL and menisci. Ruptured ACLs were debrided and torn menisci were treated with arthroscopic partial meniscectomy. Immediately following joint inspection the TPLO was performed. All surgeries were performed by the principal investigator and specific attributes of the surgical procedure were standardized for all dogs. This included using the same TPLO saw

blade in all dogs, consistent saline irrigation during osteotomy performance, and use of the same locking titanium bone plates and screws in all dogs.

After the osteotomy was made it was distracted to enable placement of the activated PRP gel or lavage with saline (Figure 2.1). In order to create the PRP gel 5,000 IU of bovine thrombin (Thrombin-JMI®, Pfizer, New York) was re-constituted with 5 ml of 10% calcium chloride solution (Ansyr™, Hospira/Pfizer, New York) to create an activation solution. The PRP was then mixed with this solution in a 10:1 ratio based upon PRP volume (PRP:activation solution) to form a malleable PRP gel, also referred to as a platelet-rich fibrin matrix (Figure 2.1)[62]. The PRP and activator were manually mixed in a sterile glass blood tube for approximately 10-30 seconds as gel formation proceeded. Approximately 90% or more of the PRP was subjectively incorporated within the fibrin gel with relatively little (less than 10%) liquid PRP releasate. The PRP gel was manually introduced into the osteotomy site at the time of surgery in all cases treated with PRP (Figure 2.1). The osteotomy site was distracted and irrigated with saline in control patients. The osteotomy was then reduced and stabilized using a commercially un-available titanium 6-hole locking TPLO plate (Arthrex Vet Systems, Naples, FL) and 1 cortical and 5 locking titanium screws (Figures 2.2 and 2.3).

Following surgery, post-operative radiographs were made to confirm appropriate surgical performance. Post-operative instructions and analgesic regime were strictly uniform for all patients with regard to several variables such as post-operative medications including that non-steroidal anti-inflammatory medications (Carprofen 4.4 mg/kg per day, Zoetis, Florham Park, NJ) were prescribed for exactly 7 days following surgery given that non-steroidal anti-inflammatory medications have been shown to influence bone healing[63]. All owners were provided with the same activity modification instructions following surgery.

Outcome measures

Dogs were re-examined, anesthetized, and radiographic, ultrasonographic, and MRI evaluations were performed at exactly 28 days post surgery. The anesthetic protocol included pre-medication with 0.005 mg/kg body weight of dexmedetomidine and 0.1 mg/kg of hydromorphone and induction with 4 mg/kg of Propofol (Zoetis, Florham Park, NJ). Anesthesia was maintained with isoflurane. Dogs were subsequently re-examined, sedated, and radiographic and ultrasonographic evaluations were performed at exactly 49 and 70 days following surgery. Sedation was obtained using 0.005 mg/kg of dexmedetomidine and 0.5 mg/kg of nalbuphine (Hospira, Lake Forest, IL).

Healing assessments

Radiography

Radiographic assessment of osseous healing was performed by one investigator (SH) who was blinded to group assignment. Radiographic scoring was based upon modification of two scoring systems previously used to assess TPLO healing[64,65]. In one of those previous studies a 10-point scale was used including assessing cortical healing on a 0-2 subscale[64]. We modified this cortical healing subscale to 0-4 as we scored cortical healing of two cortices on each of the medial-lateral and posterior-anterior radiographic views. With this modification the maximum cortical bone healing subscale was 4 and the total maximum healing score could be 12. Another study that evaluated bone healing following TPLO graded healing from 0-4 (0% healed, 1-25% healed, 26-50% healed, 51-75% healed, and 76-100% healed) based upon a medial-lateral radiographic projection alone[65]. We used the same scoring system but graded both orthogonal radiographic views and calculated the mean of these 2 scores.

Ultrasonography

Ultrasonographic assessments of osseous healing were performed by one investigator (EB) using a portable ultrasonography unit (Noblus, Hitachi Aloka Medical, Ltd.) and a linear array transducer (L64, 18-5 MHz; Figure 4). Evaluation locations included the craniomedial, caudomedial, craniolateral, and caudolateral aspects of the proximal tibia and osteotomy. Still images and cine clips of the ultrasound exam were saved. At the conclusion of the study, all patient identification information was removed from the images and cine clips to mask group assignment to the reviewer (EB). Subsequently, the same ultrasonographer evaluated cortical continuity using B-mode ultrasonography and it was scored similarly to radiography, using a 0-4 scale with a score of four representing continuous cortices at all four of the aforementioned anatomic locations. Callus formation was also assessed using B-mode ultrasonography and graded on a 0-4 scale (0=absent, 1=minimal, 2=moderate, 3=remodeled, 4=healed) using methodology that has previously been validated for use in dogs when assessing fracture healing[66-69]. Power Doppler ultrasonography was used to evaluate healing using a 0-3 scale, based upon the color and vascular density (area in mm^2) as has been previously described for assessing canine fracture healing (Table 2.1)[69].

MRI

Dogs were placed in dorsal recumbency, with the affected leg placed in a knee coil (Siemens Tx/Rx 15-Channel Knee Coil) with the stifle flexed to about 120°. Images were obtained using a 3T MRI unit (Siemens Magnetom Skyra 3T, Erlangen, Germany) and using the parameters specified in Table 2 (Figure 2.6). Images were subsequently evaluated using Osirix version 6.5.2 (Bernex, Switzerland). The sagittal plane intermediate-weighted (IW) Dixon FS and dorsal plane T1-weighted (T1w) sequences were used simultaneously for region of interest (ROI) placement

and to ensure no cortical or soft tissue partial volume averaging occurred within the ROI. Square ROIs (75mm^2 area) were drawn on the sagittal plane images spanning the osteotomy (Figure 2.6). Values for the mean pixel intensity within the ROI were recorded. This process was repeated on 3 sagittal plane images that corresponded to the most medial, central, and most lateral portions of the proximal tibial medullary bone. Care was taken to ensure the most medial slice was not affected by perceptible metal artifact. The ROI evaluation of the T1w sagittal plane images was performed after the IW images using the same methods.

Statistical analysis

Age and body weight of dogs in the two groups were compared with unpaired t-tests. Gender distribution between the two groups was compared using a Fisher's exact test. The effect of treatment on radiographic and ultrasonographic assessment of bone healing were evaluated in two ways. First, for each of the radiographic and ultrasonographic scoring systems, differences between the two treatment groups were compared at each time point using a one-tailed t-test and a p-value set at 0.05 *a priori*. These analyses were done with the radiographic 5-point and 12-point scales and the ultrasonographic assessments of cortical bone healing, callus formation, and power Doppler analysis. Similarly, evaluation of the MRI-assessed outcomes (IW Dixon and T1w TSE images) were assessed using one-tailed t-tests with a p-value set at 0.05.

Evaluation of the radiographic and ultrasonographic data were also performed using a repeated measures analyses of covariance. The initial models included the explanatory variables dog age, body weight, gender (all dogs were neutered except for one intact female dog and so all dogs were classified as just male or female), time (4, 7, 10 weeks), treatment (PRP or control), and the interaction terms treatment-by-time, weight-by-time, and age-by-time. Non-significant

interaction terms were eliminated in a backward fashion if the p-value exceeded 0.75 until a final model was obtained.

RESULTS

Data were obtained and included in analyses for 60 dogs. All data from 4 dogs were excluded from statistical analyses because they did not return for follow-up (n=1), had PRP that did not form a gel because it was activated with calcium chloride only and no thrombin was used in the activation (n=1), had a fibular fracture recognized at the 4 week recheck (n=1), or had an increase in tibial plateau angle (posterior tibial slope) from 5° to 13° at the 4 week re-evaluation consistent with mechanical instability (n=1). Three of these dogs had PRP placed at the time of surgery and 1 of these dogs was in the control group. One dog had MRI data excluded from analysis, but radiographic and ultrasonographic data were included, because the MRI unit was dysfunctioning on day 28 post-surgery and the values from the MRI analysis were dramatically different than values from all other 59 dogs.

There were no differences in age (p=0.15), body weight (p=0.83), or gender distribution (p=0.99) between dogs in the PRP and control groups (Table 2.3). Twenty-seven dogs were treated with PRP and 33 were included in the control group.

The prepared PRP had an average platelet concentration of $1.37x10^6$ platelets/µL ($\pm 489x10^3$), a leukocyte concentration of $5.45x10^3$/µL ($\pm 3.5x10^3$), and a negligible red blood cell concentration. This represented a mean 7.4X increase in platelet concentration above the baseline whole blood from which the PRP was prepared and a mean 1.1X increase in leukocyte concentration above the baseline whole blood sample. The average volume of PRP prepared and placed in the osteotomy was 4.9 mls.

All 60 dogs had successful outcomes based upon subjective assessment criteria previously established for veterinary patients[70]. All dogs had progressive healing over time based upon radiography (Tables 2.4 and 2.5) and ultrasonography (Tables 2.6-8). Radiographic scores for healing were numerically greater at all time points (4, 7, 10 weeks) for the PRP treatment group using the 5-point (Table 2.4) or 12-point scales (Table 2.5). Using the one-way t-test, there was significantly greater healing for the PRP treated group at 7 weeks (1.01 ± 0.6, $p=0.04$) and at 10 weeks (0.94 ± 0.58, $p=0.05$) using the 12-point radiographic scale. All other radiographic, and ultrasonographic assessments failed to provide a statistically significantly difference using one-tailed t-tests (Tables 2.2-6). Similarly, there were no significant differences between the two treatment groups based upon the MRI evaluation using either the IW Dixon ($p>0.05$) or T1 TSE ($P>0.05$) images (Table 2.9).

Based upon the repeated measures analysis of covariance both time (4, 7, or 10 weeks post-surgery; $p<0.0001$) and dog age ($p<0.001$) were significant predictors of radiographic healing using either the 5-point or 12-point scales. Body weight, gender, and treatment group (PRP versus control) all failed to have a significant effect ($p>0.05$) on radiographic assessment of healing. Similarly, time was a significant explanatory variable on ultrasonographic assessment of cortical healing ($p<0.0001$), callus formation ($p<0.0001$), and based upon power Doppler analysis ($p<0.0001$). Age, bodyweight, gender, and treatment did not have a significant effect ($p>0.05$) on any of these ultrasonographic outcome measures. The explanatory variables and their associated p-values are shown in Table 10.

DISCUSSION

There are few studies assessing the effects of PRP on long bone healing in dogs[56,71,72]. One study showed a benefit in a radial gap model based upon radiographic and histologic assessments[72].

They used a population of dogs that was homogenous in body weight but varied in breed and there was no reporting on age of the animals or the effect of age on bone healing[72]. Conversely, another study failed to find a beneficial effect of PRP in combination with calcium phosphate granules in an ulnar defect model in six beagles[71]. A third study presumably failed to identify a benefit of PRP combined with hydroxyapatite in a radial gap model stabilized with bone plates[72]. Given these discrepant results the effects of different PRPs on bone healing in canine models of long bone healing has remained unclear.

This study evaluated the effect of PRP on bone healing in a heterogeneous group of client-owned dogs with a commonly performed surgical procedure. The one-tailed t-tests demonstrated significantly greater 12-point radiographic healing at 7 and 10 weeks with use of PRP. However, the repeated measures analysis of covariance provided a more thorough analysis of explanatory variables that might have affected outcome using the radiographic and ultrasonographically acquired data. Those analyses showed that the only significant predictors of outcome were time since surgery and patient age. Even though there was not a significant difference between the two treatment groups with regards to body weight, gender, or age, the mean age of patients in the treatment group was slightly less than that in the control group. As a result, it seems likely that the small, and potentially clinically irrelevant, differences in radiographic scores seen between the two treatment groups at the 7 and 10 week time points was likely attributable to small differences in patient age rather than use of PRP. Accordingly, we reject our hypothesis that use of this specific PRP formulation would speed bone healing in dogs treated with a high tibial osteotomy.

With the aforementioned conclusion stated, it is worth considering the attributes and limitations of this study. This was a well-controlled study with a substantial number of dogs, the

dogs treated in this study are similar in age and weight to those dogs typically treated with TPLO[59], and that the statistically insignificant (or marginally significant) differences in radiographic healing scores between the two groups were small at all time points. Further, significant effects of time since surgery and age (radiographically) were detected for all radiographic (5-point and 12-point) and ultrasonographic (cortical, callus, and power Doppler) measures of healing. Given that both time since surgery and animal age are biologically plausible explanatory variables affecting bone healing, these results provide some evidence that the outcome measures were valid in addition to being derived from clinically relevant modalities. In turn, we do not believe that the outcome measures were insensitive. We also do not believe that this study was underpowered by an insufficient number of dogs and that use of a greater number of dogs would elucidate a clinically relevant benefit of this type of PRP for dogs treated with TPLO. Rather, we conclude that PRPs with similar characteristics to the PRP used in this study are unlikely to have a clinically relevant benefit on bone healing in dogs treated with TPLO.

There are several possible reasons that this study failed to provide evidence of augmented bone healing using PRP. One possible explanation for the lack of a significant treatment effect is that the elution of anabolic growth factors from activated PRP gels are transient[73]. Visser *et al.* (2010) demonstrated that elution of transforming growth factor-β1 eluted from canine platelet-rich fibrin membranes and matrices was greatest within the first 24 hours and was essentially negligible by 5 days[62]. Using the specific PRP production and activation methodology as was used in this study, we similarly identified that elution of both TGF-β1 and PDGF-BB was greatest in the first 24 hours and substantially lower by day 3 in vitro and virtually negligible by day 5 (data not shown). As a result, the possible benefits of PRP on bone regeneration may be hampered by fleeting delivery of anabolic growth factors. Either repeated delivery of growth

factors from PRP or development of methods to sustain anabolic growth factor release may be beneficial in enhancing the efficacy of PRP on bone regeneration[73].

A second possible reason that this study did not provide evidence of enhanced bone healing with use of PRP is that we performed a high tibial osteotomy that results in substantial bone apposition. With substantial bone apposition osseous healing proceeded uneventfully in the control group. Further, the lack of a gap probably mitigates identification of enhanced bone regeneration, which can be visualized more easily within a gap or defect[72]. Likewise, we obtained no histologic or mechanical data to assess the effects of PRP as these were client-owned dogs. Although these latter outcomes measures may increase the possibility of detecting a significant difference between groups they are not clinically applicable, whether in dogs or people.

A third possible explanation for an inability to identify a treatment effect is that we used a heterogeneous population of study subjects. This characteristic of the study potentially decreased sensitivity in comparison to if an experimental study were performed in which breed, age, weight, and gender were uniform using a population of purpose-bred research dogs. However, the inclusion of clinically-relevant heterogeneity is also a desirable characteristic of this study as it provided a relevant representation of clinical practice in which heterogeneity exists, whether treating canine or human patients. Furthermore, any lack of sensitivity associated with possible inter-individual heterogeneity was likely mitigated to some degree by inclusion of a substantial number of study patients.

A fourth possible reason for failure to augment bone healing could pertain to the specific PRP that was used in this study. At least two studies have demonstrated that the concentration of calcium in collagen gels and PRP scaffolds affect mouse osteoblast and human umbilical stem

cell viability with higher concentrations of calcium having negative effects on cellular viability[74,75]. Specifically, use of 10% calcium chloride solution combined with PRP in a 1:10 ratio were associated with less umbilical stem cell viability than use of a lower concentration (2.5%) of calcium chloride with the PRP scaffold[75]. In this study, we used 10% calcium chloride combined with thrombin in a 1:10 ratio for PRP activation, similar to the higher concentration used in the aforementioned study[75]. In addition, bovine thrombin is known to induce immune or inflammatory reactions in people and rodents[76]. The use of bovine thrombin in this study may have induced an immune or inflammatory response that could have precluded benefit with use of the PRP. Further, high platelet concentrations in PRP are not always beneficial and some studies have shown that higher platelet or growth factor concentrations are detrimental to tendon and bone healing[77,78]. We used PRP with a high platelet concentration and this may have precluded any benefit of such treatment.

Although the results of this study fail to demonstrate a benefit of bone healing, it is important to not extrapolate these results to conclude that PRP cannot have any positive effect on bone regeneration. Conclusions made based upon studies of PRP should remain specific to the species studied, the medical condition or model in which the investigation was performed, the characteristics of the PRP, and with consideration to the outcome measures used. While understanding those guidelines and the inability to draw definitive conclusions that extrapolate to other species, but also considering the possible translational relevance of this canine model, these data do not support investigation of a similar human PRP production in conjunction with a well-apposed and rigidly stabilized osteotomy in people, such as a closing-wedge high tibial osteotomy. This latter conclusion is obviously tenuous because this study was performed in dogs and not people. However, these results and this latter conclusion is at least consistent with

numerous clinical studies in people that fail to identify a positive effect of PRP on bone healing, even when open fracture gaps and open osteotomies are considered[55]. Rather, further studies should likely be performed in relevant models or human clinical populations in which bone loss, fracture gaps, or delayed union are present so as to optimize the likelihood of identifying a treatment effect.

CHAPTER 3

RADIOGRAPHIC, ULTRASONOGRAPHIC AND MAGNETIC RESONANCE IMAGING EVALUATION OF BONE HEALING IN DOGS RECEIVING TIBIAL PLATEAU LEVELING OSTEOTOMY WITH TITANIUM SURGICAL IMPLANTS[2]

[2] Emily E. Burke, Samuel P. Franklin, Shannon P. Holmes. To be submitted to *Veterinary Radiology and Ultrasound.*

ABSTRACT

Objectives

The purpose of this study was to investigate and compare the efficacy of radiography, ultrasonography and magnetic resonance imaging to evaluate bone healing in dogs receiving tibial plateau leveling osteotomy.

Study Design

Randomized controlled trial

Methods

Fifty-nine client-owned pet dogs with naturally occurring rupture of the anterior cruciate ligament were treated with a tibial plateau leveling osteotomy. All dogs had the osteotomy stabilized with identical titanium alloy implants and all aspects of the surgical procedure and post-operative care were identical among dogs of the two groups. Bone healing was assessed at exactly 28, and 70 days after surgery using radiography and ultrasonography and using MRI at day 28. Pearson's correlation tests were used to identify whether grades for MRI correlated with radiographic grades for healing at 70 days after surgery.

Results

Fifty-nine dogs completed the study. All dogs demonstrated progressive healing over time and achieved clinically successful outcomes. There was no correlation between magnetic resonance imaging grades at 28-days post-op and radiographic grades at 70 days post op.

Conclusion

MRI and ultrasonography are feasible and clinically useful adjunctive imaging modalities for monitoring of osseous healing post-op. Radiography remains clinically relevant as an affordable and reliable method of post-operative monitoring.

INTRODUCTION

Cranial cruciate ligament (CrCL) rupture is the most common cause of hindlimb lameness in dogs, with an estimated 1.2 million surgeries performed in the United States annually to treat this condition[1]. Tibial plateau leveling osteotomy (TPLO) is the most common technique used by veterinary surgeons to provide mechanical stability to the stifle joint in dogs affected with CrCL rupture[57]. Steel bone plates and screws are typically used and, along with appropriate surgical technique, provide stabilization of the osteotomy site as the bone heals; a process that typically takes 8-12 weeks[65].

Radiography is the most commonly used imaging modality for evaluating osseous healing in the weeks following surgery[2]. For adequate evaluation of fracture, such as with an osteotomy, two orthogonal views are essential, with oblique views sometimes required in order to identify subtle changes[2]. For post-operative evaluation of the stifle, the caudocranial and mediolateral projections are most commonly utilized [79 80]. These projections are centered on the femorotibial joint with a field of view wide enough to include the tarsus. Despite its utility and excellent spatial resolution, radiography is limited in assessing osseous healing in that relevant anatomy can be obscured by surgical implants, and there is no assessment of metaphyseal healing or vascularity. Additionally, radiographic evidence of osseous change is not immediately conspicuous after injury[81]. This is due to the poor contrast resolution of the modality and inherent inability to detect the minor differences in mineral composition experienced during the healing process.

Because of limitations with assessing osseous healing with radiography, several studies have investigated the potential utility of ultrasound as an adjunct for evaluating osseous healing[66,68]. Purported advantages of ultrasonography include its superior provision of cross-

sectional anatomy as well as contrast resolution compared to radiography. Brightness mode (B-mode) ultrasonography provides qualitative information about soft tissue callus formation and osseous remodeling during fracture healing. It is a more sensitive identifier of the amount of callus present across a fracture line compared to radiographs, leaving some to conclude that radiographs underestimate the degree of fracture stability [66,82]. Adequate vascular supply is a critical component to normal osseous healing after fracture [83] [81] [2]. The addition of power Doppler to an ultrasound exam provides information about the vascularity of the fracture site and surrounding soft tissues[69]. Compared to color Doppler, power Doppler is more sensitive to the presence of blood flow even in low velocity areas. Though it does not provide information about the direction of blood flow, it is favored for identifying the presence of blood flow in smaller vessels [84]. Multiple studies have suggested that the combination of B-mode ultrasonography and power Doppler ultrasonography predict clinical union and osseous healing more quickly than does radiography[66,68,69].

Magnetic resonance imaging (MRI) is another diagnostic modality that has several possible advantages over both radiography and ultrasonography for monitoring osseous healing. MRI has superior soft tissue contrast resolution compared to other diagnostic imaging modalities [4], which is why it has become the gold standard in human musculoskeletal evaluation[3]. With respect to fracture healing, it has the ability to evaluate osseous sclerosis, hyperintensity and perfusion within osseous structures, as well as morphologic and physiologic changes in the surrounding soft tissue structures. Recently, there is increasing clinical use of MRI for assessing bone healing, but the available data is limited when compared to other methods of assessing fracture or osteotomy healing [36,85,86]. This may be due to expense, availability, expertise or more likely the artifact issues associated with surgical implants. The development of MR sequences that

suppress these implant-associated artifacts has made MR imaging of fracture healing a possibility.

The purpose of this study was to compare radiography, ultrasonography and MRI evaluation of bone healing in dogs after TPLO. We hypothesized that MRI evaluation at 4 weeks (w) post-operative would strongly correlate with radiographic scores of bone healing at 10w post-op.

METHODS

Sixty-four client-owned dogs were enrolled in this prospective, blinded and randomized clinical study. The inclusion criteria were a diagnosis of naturally-occurring CrCL rupture made through a combination of orthopedic examination and standard pre-operative stifle radiography. Additionally, each dog was deemed to be clinically normal aside from their CrCL rupture as determined from clinical history, physical exam, and blood work (complete blood count and serum chemistry). All dogs were required to be 2-10 years of age and >25 kilograms.

Arthroscopic evaluation of the joint was performed to enable confirmation of CrCL rupture, debridement of the ruptured portion of the CrCL, and for identification and treatment of meniscal damage. Immediately following joint inspection, a TPLO was performed using standard technique. The TPLO was stabilized in all cases using custom titanium bone plates and screws. One board-certified surgeon (SPF) performed all surgeries, utilizing the same instruments and locking titanium bone plates and associated screws for each patient. Mediolateral and caudocranial radiographs of the affected limb were obtained immediately post-operatively in order to evaluate surgical technique, which is considered standard of care. Each patient was discharged 24-36 hours after surgery with the same routine post-operative instructions for activity limitation, physical rehabilitation, and medication regimen which

included non-steroidal anti-inflammatory medications (Carprofen 4.4mg/kg bw per day, Zoetis, Florham Park, NJ) prescribed for the 7 days following surgery.

Diagnostic imaging evaluations were performed exactly 28 and 72 days (4 and 10 weeks) after surgery for each patient. At the 4w recheck, dogs received a thorough orthopedic examination prior to being anesthetized. The anesthetic protocol utilized for the 4w recheck included premedication with dexmedetomidine (0.005 mg/kg bw) and hydromorphone (0.1mg/kg bw) administered intramuscularly, followed by induction with Propofol (4 mg/kg bw, Zoetis, Florham Park, NJ). Anesthesia was maintained with isoflurane. Immediately following anesthetic induction radiographic, ultrasonographic and high-field MR images were obtained. At the 10w recheck, dogs were sedated and radiographic and ultrasonographic images were obtained. Sedation protocol included intravenous administration of 0.005mg/kg dexmedetomidine and 0.5 mg/kg nalbuphine (Hospira, Lake Forest, IL).

Imaging Assessments

Radiographic studies at all evaluation time points consisted of mediolateral and caudocranial projections of the tibia, centered on the femorotibial joint with the field of view widened to include to tarsus in both views. One reviewer (SPH) blinded to all clinical aspects of the bases evaluated the 4w and 10w radiographs over multiple one hour review sessions to avoid imaging fatigue. Two grading systems were to assign scores of osseous healing for each patient, based upon systems described previously to assess healing after performance of TPLO[64,65]. Our modifications resulted in a single system for grading cortical osseous healing on a 0-4 subscale, resulting in a maximum score of 12 from four different categories: cortical continuity, conspicuity of the osteotomy, subjective callus formation or remodeling, and degree of rounding at the distal step of the osteotomy. The second grading system was more qualitative with healing

graded on a 0-4 scale (0% healed, 1-25% healed, 26-50% healed, 51-75% healed, and 76-100% healed). This grading scale was modified from one described previously[65] to include both radiographic projections, with a mean score calculated.

Ultrasonographic studies were performed by a single investigator (EB) utilizing a portable ultrasonography unit (Noblus, Hitachi Aloka Medical, Ltd.) and linear array transducer (L64, 18-5 MHz). The patient was positioned in lateral recumbency with the affected limb up. The stifle was clipped and cleaned with alcohol prior to application of coupling gel. Still images and cine loops were obtained at a maximum depth of 2 cm in B-mode in four locations: the craniomedial, caudomedial, craniolateral and caudolateral aspects of the proximal tibia and osteotomy site. Power Doppler images were then obtained in the same locations. Static images were obtained immediately craniomedial and caudomedial to the implant, as well as on the cranio- and caudolateral surfaces of the tibia. Medially, cine loops were made to globally evaluate the bone and changes in the surrounding soft tissues from the level of the implant cranially to the tibial tuberosity (for a total of 90° of evaluation) and from the implant to the visible margin of the caudal tibia (for a total of 90° of evaluation). Similar techniques were used for acquisition of the laterally-oriented cine loops.

Each MRI exam was performed on the same 3T MRI unit (Siemens Magnetom Skyra 3T, Erlangen, Germany). The patients were placed in dorsal recumbency with the affected limb in a knee coil (Tx/Rx 15-Channel Knee Coil, Siemens, Erlangen, Germany) such that the stifle was flexed to approximately 120°. Sequences acquired included T2-weighted(w) DIXON, T2w anatomical and T1w Turbo Spin-Echo (TSE) in the sagittal plane, as well as a proton density-weighted (PD)w sequence in the dorsal plane. A sagittal, pre-contrast T1w TSE centered on the osteotomy and with a smaller field of view (FOV) was additionally acquired (Table 3.2); this

image provided the mask for the dynamic contrast enhanced images. Immediately following initiation of contrast administration (dimeglumin gadopentetate; Magnevist; Schering, Berlin, Germany) (0.1 mmol/kg/body weight), acquisition of 25 consecutive dynamic contrast enhanced (DCE) measurements were performed with 34.8 seconds (sec) between each measurement. The same smaller-FOV T1w TSE sequence was utilized.

Post-processing analysis of the sequences was performed by the same investigator (EB) using commercially available software (OsiriX V6.5.2, Bernex, Switzerland). Square regions of interest (ROI; 75 mm^2 area) centered on the osteotomy site were drawn at three locations on the sagittal plane images: the most medial slice possible without interference from metal artifact, the exact middle, and the most lateral slice possible without interference from local soft tissue structures. Each ROI spanned the osteotomy site to include portions of both the proximal and distal tibial segments. Values for the mean pixel intensity within the ROI were recorded. This process was repeated for the T2w DIXON, T2w Anatomical and T1w TSE sagittal images. For the PDw dorsal-plane images, a rectangular ROI (75 mm^2 area) was drawn, spanning the length of the osteotomy without including the tibial cortices. Values for the mean pixel intensity within the ROI were similarly recorded.

The same software was used for analysis of the DCE MRI images [86]. For each time period, the slice corresponding to the center of the osteotomy site was analyzed. A free-hand ROI was drawn to span the entire length of the osteotomy and including trabecular bone immediately adjacent to it. The ROI was propagated through each time point in order to acquire data from the same region over time. The mean for each ROI at each time point was recorded. The area under the curve (AUC) was calculated for each patient.

Statistical Analysis

Pearson's correlation tests were performed to determine whether MRI scores correlated with 4w and 10w ultrasonographic and radiographic grades.

RESULTS

Of the sixty-four dogs originally enrolled, fifty-nine dogs completed all aspects of the study and had complete radiographic, ultrasonographic, and MRI evaluations performed. Four dogs were excluded due to the development of post-operative complications (n = 3) or did not return for follow-up (n = 1). One additional dog was excluded due to an incomplete MRI examination.

At 4w post-op, 47/59 dogs (80%) had a clearly visible osteotomy line. This number decreased to 10/59 dogs (17%) by the 10w post-op evaluation. There were no patients with complete osseous healing observed at 4w post-op using either radiographic scale. At 10w post-op, five dogs were considered completely healed when the 12-pt scale was used, and none when the 5-pt scale was used (Table 3.3). The individual grade for radiographic subjective formation of callus at 4w post-op had a weak positive correlation with the final grade for osseous healing at 10w post-op using the 12-pt scale ($R^2 = 0.12$).

Bone plates were identified as hyperechoic linear surfaces parallel to and obscuring the cortical bone margins on the medial aspect of the tibia. Each exam took an average of 15 minutes to complete. The images were assessed at the completion of the project by the same investigator (EB) using anonymized images. B-mode ultrasonography was utilized to evaluate cortical continuity on a 0-4 scale similar to the scoring system used for radiographic assessment, with a score of 4 representing continuous cortices at each of the four locations imaged (Figure 3.3). Callus formation was assessed utilizing a 0-4 scale (0 = absent, 1 = minimal, 2 = moderate, 3 = remodeled, 4 = healed) previously described for evaluation of fracture healing in dogs (Table

3.4). Grading of the power Doppler images consisted of a previously validated 0-3 scale, based on vascular density (area in mm^2) and signal color (Table 3.1).

The MR images were consistently considered to be of excellent diagnostic quality for each MR imaging series in each patient, with no artifacts detected that would corrupt quantitative evaluations with one exception. Signal void caused by the presence of the titanium surgical implants were limited to within the 2-4mm of tissue immediately adjacent to the implants for the T2 DIXON, T1w TSE, DCE, PDw and T2 Anatomical studies for all but one patient. In that patient, artifact caused complete obliteration of the osteotomy site for the T2 Anatomical study alone.

When comparing the various quantitative MR assessments to radiographic grades of osseous healing at 4w post-op, weak positive correlations were identified between parameters. Scores for ROI signal intensity on the T2w DIXON sequences were positively correlated with radiographic grades using both the 5-pt and 12-pt scales ($R^2 = 0.12$ and 0.09, respectively). This weak correlation between T2w DIXON ROI measurements and radiographic grades for osseous healing using the 12-pt scale was also observed at 10w post-op, ($r = 0.16$, $R^2 = 0.03$). When compared to the 4w post-op ultrasonographic exams, the T2w DIXON ROI measurements had a weak positive correlation with grades for cortical continuity ($R^2 = 0.08$). The T1w TSE ROI scores were weakly, positively correlated with the power Doppler grade for number of signals at 4w post-op ($R^2 = 0.07$). No other correlations were observed between any MRI sequence and grades for radiographic and ultrasonographic osseous healing at 4w or 10w post-op.

DCE MRI data was available for 58 dogs. One dog was excluded due to a radiofrequency breach during image acquisition, resulting in substantial image artifact. For each patient, signal intensity over the region of interest had an initial linear increase, which plateaued and persisted

throughout the remaining time points (Figure 3.2). No significant signal washout was appreciated over the time frame during which the study proceeded. For each patient, a >10-fold increase in signal intensity compared to the pre-contrast image was observed within the region of interest. There was no correlation between the calculated values for area under the curve (AUC) and radiographic grades of osseous healing at 10w post-op using either grading scale ($r < 0.01$).

DISCUSSION

Ultrasonography and high-field magnetic resonance imaging of the canine stifle following TPLO with titanium implants are clinically feasible imaging techniques for evaluation of osseous and soft tissue healing. Routinely, orthogonal radiographs are performed immediately post-operative and used as a baseline for future evaluation [2]. Images obtained in the weeks after surgery should be made with significant consideration for patient positioning and implant angulation that matches the initial images as closely as possible [2]. Though procedurally more time consuming, the effort allows for identification of post-operative complications such as implant loosening and changes in tibial plateau angle, both of which jeopardize the integrity of the surgically established joint mechanics. In 80% of the patients enrolled in this study, a visible widening of the osteotomy site was observed radiographically at the 4w recheck. The same finding was observed in only 47% of dogs during MRI examination. Widening of a fracture line in the 3-4 weeks immediately post-op is considered a normal finding, representing the cellular turnover necessary for callus formation and mineralization [83 81 2]. The 33% of dogs with radiographic evidence of fracture widening that wasn't appreciated with MRI likely represent cases in which the "gap" was filled in with connective tissue scaffolding not yet mineralized. The radiographic interpretation of low incidence of complete or near-complete osseous at this recheck was expected based on the previously published times for complete osseous healing of

8-12w after fracture[65].

Digital radiography has inherently better spatial resolution compared to ultrasonography and magnetic resonance imaging. This gives radiography an advantage in the ability to differentiate between smaller adjacent structures. Though it is the most commonly utilized imaging modality for monitoring of osseous healing after fracture repair in our veterinary patients, there are some instances in which clinically suspected fractures remain inconspicuous on radiographs [81]. For these patients, early callus formation identified 7 to 10 days after injury can be the only way to confirm a diagnosis. In this study, B-mode ultrasonography consistently provided lower grades for evaluation of cortical continuity compared to radiographic evaluation. This is suggestive of a more sensitive ability to identify cortical integrity using ultrasound, and represents one area in which ultrasound proves superior to radiography. Although not specifically evaluated, the superior soft tissue contrast resolution in MR images would be expected to perform similarly to ultrasound.

One of the most important stages of bone healing after injury is in the re-establishment of an appropriate vascular supply. During performance of an osteotomy, the surgeon disrupts the normal blood supply for both segments of bone created. Adjacent soft tissue structures provide extraosseous blood supply to deliver necessary nutrients and oxygen to the affected bone [83]. This form of neovascularization can be monitored via power Doppler ultrasonography and is expected to disappear as the medullary vascular supply is restored. Inclusion of power Doppler ultrasonography in our post-operative exams proved clinically feasible and repeatable, with the total exam time lasting no longer than 15 minutes. Images used for interpretation were selected based on maximum color signal, whilst avoiding using images immediately adjacent to the implant due to previously described false positive signals[68]. Though the power Doppler scores

for the cranial aspects of the osteotomy site (both medially and laterally) were numerically higher than those for the caudal aspects, the lack of a statistically significant difference between scores makes this detail difficult to interpret. As the caudal static images and cine loops were technically more difficult to obtain, it is possible that user error may have played a roll. Additionally, this study failed to identify a statistically significant correlation between power Doppler assessment at 4w post-op and radiographic grades of osseous healing at 10w post-op. This makes it difficult to recommend as a predictive imaging modality for the identification of patients which will experience delayed healing.

MRI has been suggested as a non-invasive diagnostic technique for stifle evaluation in dogs who have undergone surgery for repair of CrCL rupture, particularly for investigation of suspected late meniscal tears[87]. Its use in human orthopedics is varied and includes evaluation of post-op complications associated with total hip arthroplasty, monitoring of healing following tissue allografts and fracture dating for forensic medicine[31,36,86]. For this study, we investigated the utility of MRI for the specific evaluation of osseous healing following TPLO with titanium plate and screw implants. Sequence selection was aimed at identifying changes in trabecular bone composition, the presence of medullary bone hyperintensity and cellular alteration of tissues, as well as differences in osseous neovascularization.

The inflammatory phase of bone healing lasts up to three weeks after injury and includes hematoma formation and the presence of bone marrow edema [81 36,83]. These two changes results in initially high values for T2 and T1 relaxation, both decreasing over time in normally-healing bone[88]. If imaged in the intermediate phases of bone healing, after the inflammatory phase but before complete remodeling and mineralization has occurred, heterogenous signal intensities can be seen. Dogs in this study exhibited a large variation in numeric values for both T1w and T2w

images. These values represented varying degrees of hyperintensity and sclerosis associated with normal osseous healing. We identified very weak positive correlations between the T2w DIXON and PDw sequences and radiographic grades of osseous healing at 10w post-op. Though no predictive statements can be made, the ability to easily evaluate osseous and soft tissue structures within and surrounding the stifle joint after performance of TPLO is invaluable. MRI cannot be considered a completely benign procedure due to the need for general anesthesia, but its utility in post-operative evaluations could be beneficial with respect to distinguishing abnormalities requiring repeat surgical intervention from those that do no.

With inadequate osseous perfusion there will be abnormal if not incomplete healing of a fracture site. Where power Doppler can provide quantitative information about the vascularity of surrounding soft tissues and the initial callous, DCE-MRI quantifies intraosseous neovascularization. Recently highlighted for its ability to predict fracture non-unions, degrees of tissue enhancement after administration of a contrast medium has been shown to accurately predict patterns of healing in human medicine[43,44]. Our findings of an initial linear increase in ROI pixel intensity followed by a plateau that persisted through the remaining time points was similar to previous work[89], indicating increased vascularity at the osteotomy site 4w post-op TPLO. In this study, we were unable to identify correlations between this quantitative evaluation of neovascularization and radiographic grade for healing at 10w post-op. Further work to investigate DCE-MRI after fracture repair in veterinary species could help to establish normal values for osseous perfusion, as well as cut-off values for detection of post-operative complications. Despite excellent surgical technique, owner compliance after discharge plays a crucial role in healing in veterinary species. Failure to appropriately restrict exercise remains a

cause of potentially catastrophic post-operative complications, and could be one explanation for our inability to predict patient healing in this study.

One consideration for the utility of post-operative orthopedic MRI is the ability to acquire diagnostic-quality images in the face of surgical implants. The magnetic susceptibility of commonly used steel implants cause significant artifact which results in geometric distortions, signal voids and signal pile-up[90]. As a ferromagnetic substance, steel has a very high magnetic susceptibility and thus can create local field inhomogeneities. Implants made of nonferromagnetic substances, such as a titanium alloy, have a much lower magnetic susceptibility and so do not affect field homogeneity as strongly. As a result of their magnetic susceptibilities, artifacts produced by metallic implants are more pronounced at higher magnetic field strengths. This is one reason lower field units are often utilized when implant status is known[31]. Specialized sequences have been developed to minimize these artifacts and are characterized by higher bandwidths, the use of view angle tilting and MR unit specific phase encoding gradient application within pulse sequences[26,32,33].

In order to facilitate high quality MRI of our patients, custom titanium bone plates and associated screws were used in conjunction with artifact suppression optimized pulse sequences commonly used in musculoskeletal imaging. For all stifles in this study, the osteotomy site was easily visualized in 5-6 consecutive slices comprising 75-80% of its total length. Variation in the shape of the proximal tibia laterally and minimal signal void due to the presence of the metallic implant medially were the primary causes of an inability to evaluate the osteotomy site in its entirety.

One limitation of this study was the single time point used for MRI data acquisition. Additional MR examinations were considered not feasible due to the inherent risk associated

with multiple anesthetic events and the expense of each MR examination. Future studies involving consecutive MR exams could provide details about the patterns of T1 relaxation, T2 decay and changes to neovascularization observed through DCE-MRI. This would potentially allow us to identify patterns associated with normal healing which could predict and manage post-operative complications.

One additional limitation is the TPLO model used in this study. The excellent apposition of tibial segments in combination with rigid fixation from the bone plate and screws favors primary osseous healing. In this method, healing and remodeling occurs simultaneously and external callus can be minimal [81]. This model was selected based on the high number of TPLO surgeries performed at our institution and nationwide, which allowed us to enroll a significant number of patients into the study with minimal effort.

In conclusion, radiography remains clinically relevant as an affordable and reliable method of monitoring post-op osseous healing. MRI and ultrasonography are feasible and clinically useful adjunctive imaging modalities for the monitoring of post-operative healing. Though we were unable to prove any predictive trends, the superior contrast resolution of MRI is highly desirable for identification of osseous and soft tissue abnormalities which may not be evident with radiography, including inappropriate metaphyseal vascularization. Further work using DCE-MRI could provide clinically useful threshold values for identification of appropriate vascularization, similar to work done for human patients [49] [43].

CHAPTER 4

CONCLUSION

For those dogs receiving tibial plateau leveling osteotomy, radiography remains the imaging modality of choice for monitoring of post-operative osseous healing. The use of titanium surgical implants facilitates diagnostic quality magnetic resonance imaging, in combination with appropriate sequence selection for minimizing inhomogeneity artifacts. Magnetic resonance imaging and ultrasonography are efficacious and feasible adjunct imaging modalities for monitoring of these patients, both offering details about vascularity and intraosseous change that cannot be appreciated with radiography alone. Though we were unable to identify correlations between MRI findings and grades of osseous healing, further work to evaluate the soft tissues surrounding fracture sites, as well as to optimize the DCE sequence, is warranted.

TABLES

Table 2.1. Power Doppler ultrasonographic scoring scheme

Category/score	0	1	2	3
Color	none	blue	red/purple	white
Vessel area (mm^2)	none	<5mm2	5-10mm2	>10mm2
Number	none	<5	5 to 10	>10

Table 2.2. MRI sequence parameters

Parameters	T1 Turbo Spin Echo (TSE)	IW DIXON
Image weighting	T1	Intermediate
Plane of acquisition	Sagittal	Sagittal
2D vs 3D	2D	2D
Echo time (TE)	9.4	79
Repetition time (TR)	591	4530
Flip angle	180	120
Number of acquisitions	2	1
Slice thickness	1.6mm	2mm
FOV and matrix dimensions	100*140 FOV, 644*896 matrix	140*140 FOV, 768*768 matrix
Imaging options	WARP on	Fat-saturated
Bandwidth	445	310
Sequence length	3:09	9:49

Table 2.3. Demographic data on dogs included in the study.

	PRP group (n=27)	Control group (n=33)	p-value
Age	4.9 years (±1.7)	5.7 years (±2.4)	0.15
Bodyweight	32.2 kg (±5.4)	31.9 kg (±4.7)	0.83
Male	0	0	0.99*
Intact Female	0	1	
Castrated Male	12	15	
Spayed Female	15	17	

Table 2.4. Summary of Radiographic Healing Scores (5-point Scale)

	4 week	7 week	10 week
Saline	1.47 (±0.65)	2.85 (±0.83)	3.58 (±0.72)
PRP	1.67 (±0.80)	2.93 (±0.85)	3.69 (±0.57)
p-value	0.15	0.36	0.26

Table 2.5. Summary of Radiographic Healing (12-point Scale)

	4 week	7 week	10 week
Saline	3.00 (±1.95)	6.06 (±2.09)	8.58 (±2.53)
PRP	3.78 (±2.19)	7.07 (±2.30)	9.52 (±1.81)
p-value	0.08	0.04	0.05

Table 2.6. Summary of Ultrasonographic Assessment of Cortical Continuity (5-point Scale)

	4 week	7 week	10 week
Saline	0.06 (±0.24)	1.12 (±0.86)	2.97 (±0.95)
PRP	0.11 (±0.32)	1.44 (±0.85)	3.30 (±0.67)
p-value	0.24	0.07	0.07

Table 2.7. Summary of Ultrasonographic Assesment of Callus Formation (5-point Scale)

	4 week	7 week	10 week
Saline	1.64 (±0.42)	2.48 (±0.51)	3.25 (±0.54)
PRP	1.74 (±0.40)	2.59 (±0.33)	3.43 (±0.35)
p-value	0.16	0.17	0.08

Table 2.8. Summary of Power Doppler Ultrasonographic Assessment (5-point Scale)

	4 week	7 week	10 week
Saline	1.45 (±0.52)	1.02 (±0.38)	0.76 (±0.37)
PRP	1.49 (±0.58)	1.08 (±0.36)	0.71 (±0.34)
p-value	0.38	0.24	0.31

Table 2.9. MRI Assessment at 4 weeks

	T1	T2 Dixon FS
Saline	223.1 (63.4)	172.0 (±64.5)
PRP	237.3 (69.7)	160.1 (±58.1)
p-value	0.41	0.46

Table 2.10. P-values associated with each explanatory variable used in a repeated measures analysis of covariance.

	Time	Age	Weight	Gender	Treatment
Radiographic Assessment					
5-point	<0.0001	0.0003	0.66	0.31	0.92
12-point	<0.0001	<0.0001	0.17	0.18	0.22
Ultrasonographic Assessment					
Cortical (5-point)	<0.0001	0.47	0.55	0.99	0.14
Callus (5-point)	<0.0001	0.21	0.96	0.36	0.26
Power Doppler	<0.0001	0.12	0.08	0.62	0.54

Table 3.1. Power Doppler ultrasonographic scoring scheme

Category/score	0	1	2	3
Color	none	blue	red/purple	white
Vessel area (mm^2)	none	<5mm2	5-10mm2	>10mm2
Number	none	<5	5 to 10	>10

Table 3.2: MRI sequence parameters

Parameters	T1w Turbo Spin Echo (TSE)	T2w DIXON	PDw	T2w Anatomic	T1w TSE DCE
Image weighting	T1	T2	PD	T2	T1
Plane of acquisition	Sagittal	Sagittal	Dorsal	Sagittal	Sagittal
2D vs 3D	2D	2D	2D	2D	2D
Echo time (TE)	9.4	79	57	13.8, 27.6, 41.4, 55.2, 69	9.1
Repetition time (TR)	591	4530	5150	1000	544
Flip angle	180	120	180	180	150
Number of acquisitions	2	1	2	5	25
Slice thickness	1.6mm	2mm	2mm	2mm	2mm
FOV and matrix dimensions	100*140 FOV, 644*896 matrix	140*140 FOV, 768*768 matrix	100*140 FOV, 644*896 matrix	119*159 FOV, 576*768 matrix	81*100 FOV, 94*128 matrix
Imaging options	WARP on	Fat-saturated		Interpolated	34.8s between acquisitions
Echo train length	4	10	21	5	5
Bandwidth	445	310	445	350	500
Time for acquisition	3:09	9:49	5:04	6:45	8:43

Table 3.3. Summary of radiographic healing scores

	4 week	10 week
12-pt Scale	3.39 (± 2.08)	9.03 (± 2.27)
5-pt Scale	1.58 (± 0.71)	3.64 (± 0.61)

Table 3.4. Summary of ultrasonographic assessment scores

	4 week	10 week
Cortical continuity	0.90 (± 0.94)	3.12 (± 0.85)
Callus formation	1.69 (± 0.41)	3.34 (± 0.47)
Power Doppler – Grade	1.45 (± 0.54)	0.73 (± 0.35)

FIGURES

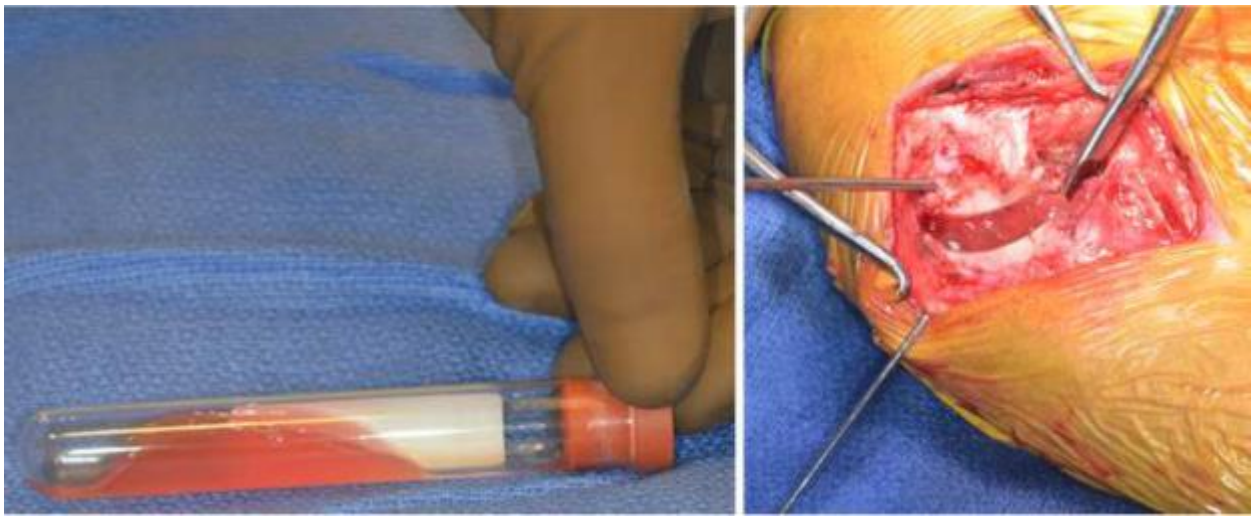

Figure 2.1. The activated PRP immediately after it has formed a malleable gel and with placement into the distracted osteotomy. Note that the osteotomy would be reduced and stabilized following distraction and PRP placement.

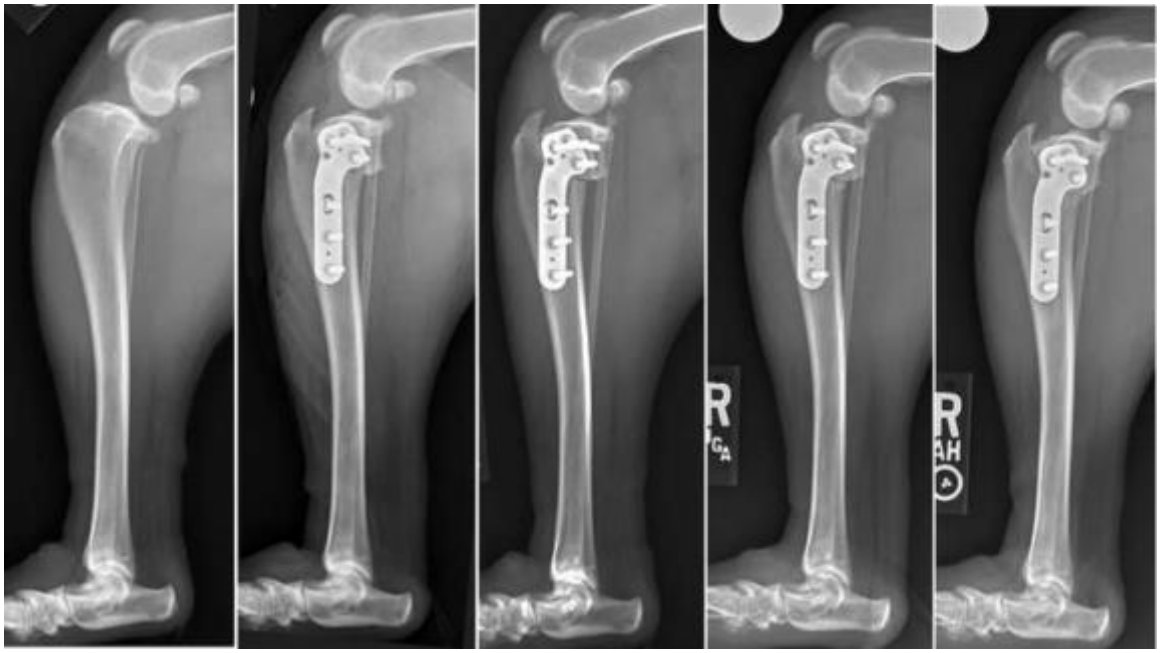

Figure 2.2. Representative medial-lateral radiographs for one dog pre-operatively, immediate post operatively, and 4, 7, and 10 weeks post operatively. Caudal femoral subluxation is apparent on the pre-operative medial-lateral view and is resolved on all subsequent medial-lateral views. The bone plate obscures approximately 50% of the osteotomy on the medial-lateral radiographic view. However, progressive radiographic healing can be seen anterior and posterior to the bone plate.

Figure 2.3. Representative posterior-anterior radiographs for the same dog as in Figure 2.2 pre-operatively, immediate post operatively, and 4, 7, and 10 weeks post operatively. Progressive radiographic healing of the osteotomy can be seen.

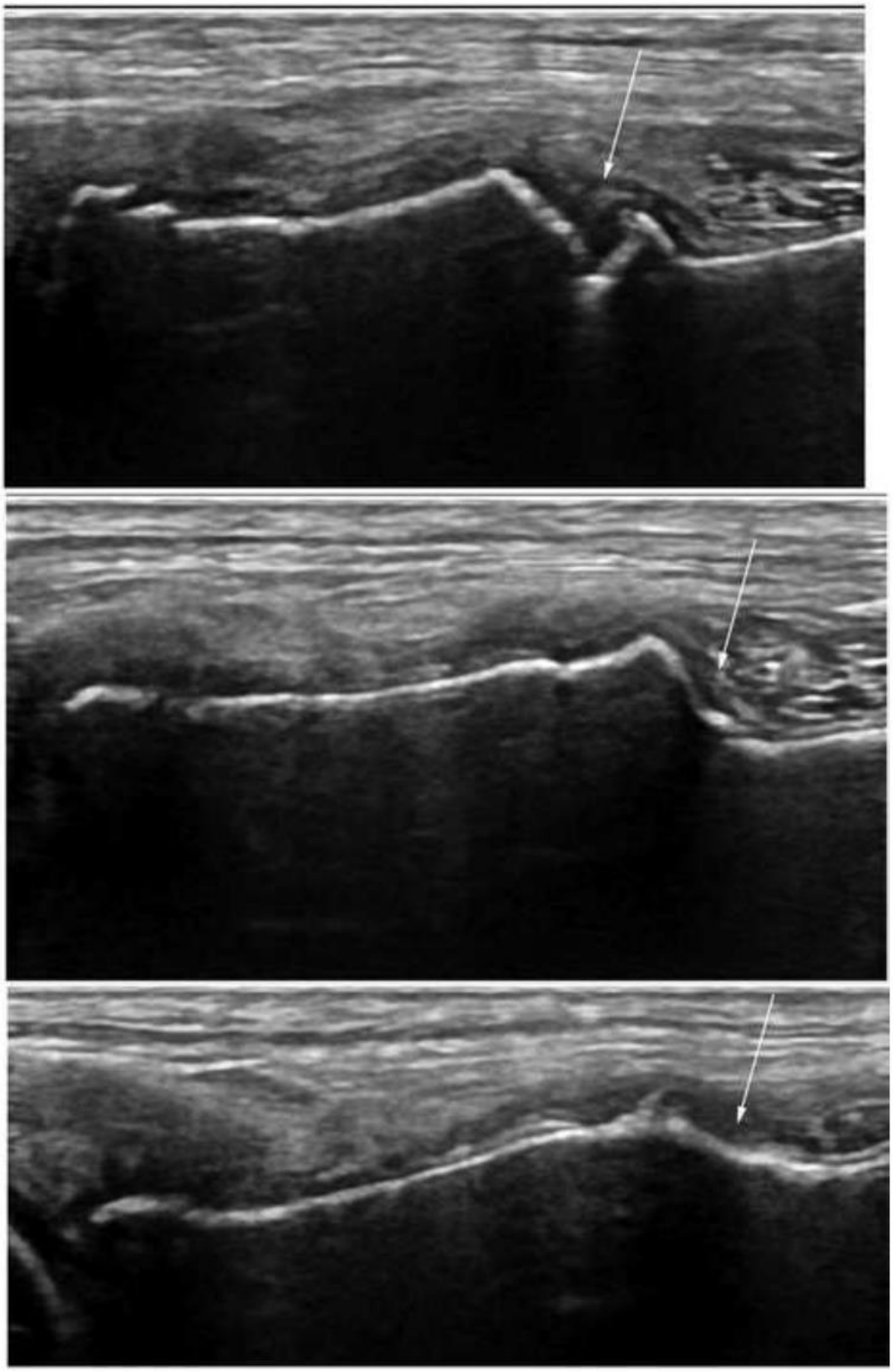

Figure 2.4. Brightness mode ultrasonographic images for one dog at 4, 7, and 10 weeks following surgery. Note the progressive healing of the osteotomy (arrows) over time.

Figure 2.5. Power Doppler ultrasonographic images for one dog at 4, 7, and 10 weeks following surgery. Note the decreasing vascular density over time (small arrows) corresponding to progressive healing of the osteotomy (larger arrows).

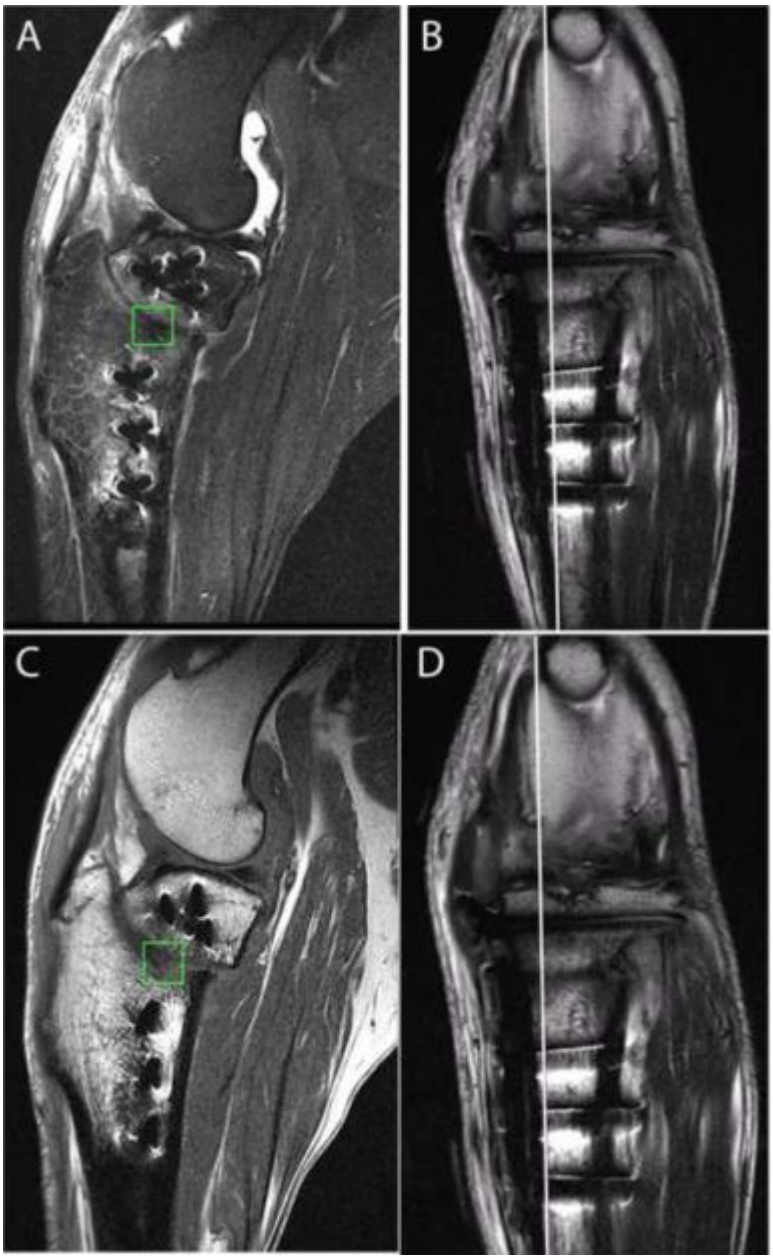

Figure 2.6. Representative MRI images used for quantitative assessment of osseous healing and showing placement of the square regions of interest on the sagittal slices and in which the intensity was measured. The corresponding white lines on the dorsal plane images demonstrate the location of the sagittal slice in which the ROI was drawn with regard to medial-lateral location. A) T2 Dixon fat suppressed sagittal plan sequence; B) Proton density weighted frontal plane sequence; C) T1 turbo spin echo sagittal plane sequence; D) Proton density weighted.

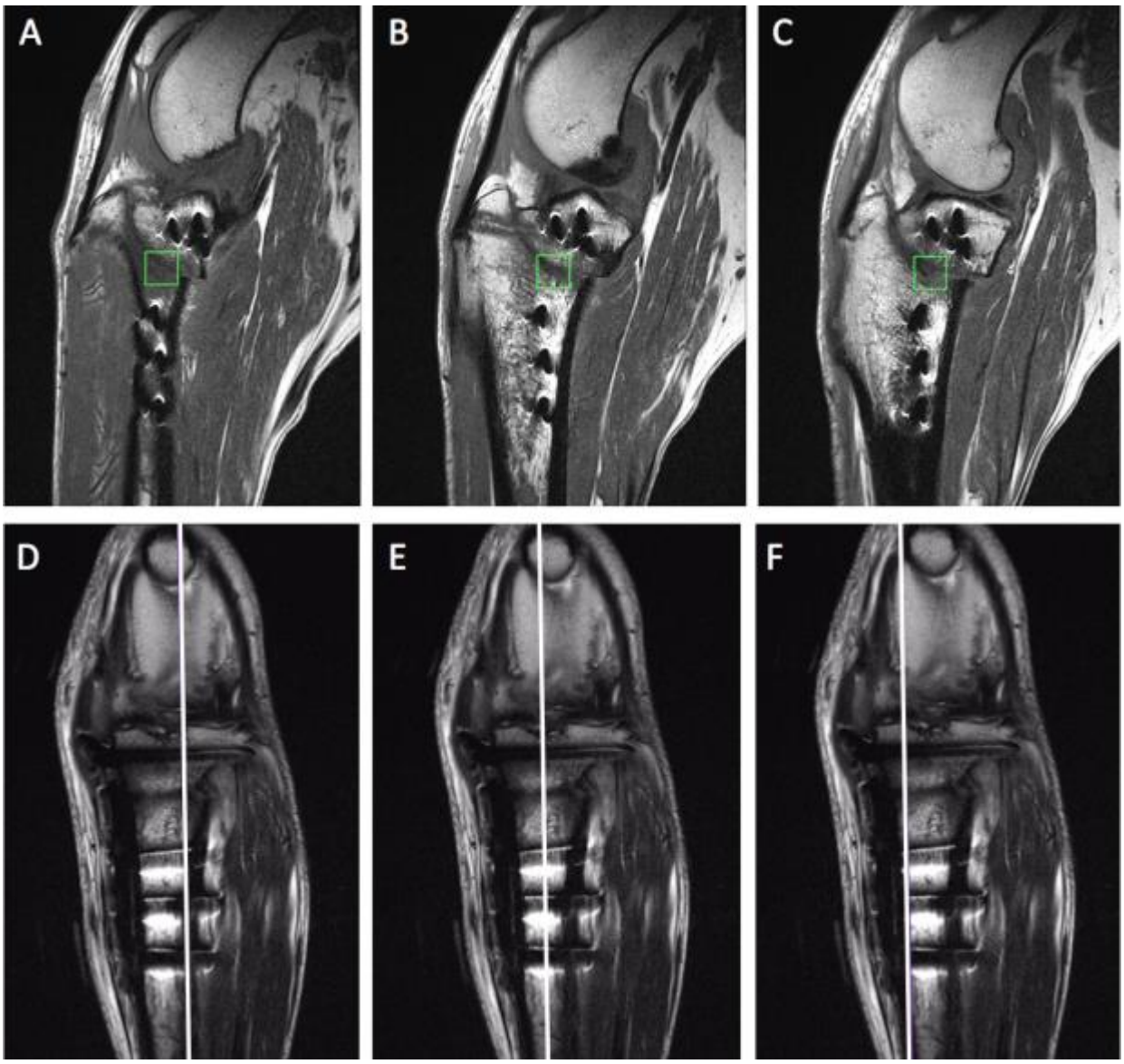

Figure 3.1. Representative MRI images used for quantitative assessment of osseous healing. Regions of interest (green boxes) are drawn on T1-weighted Turbo Spin Echo sagittal images for the lateral (A), middle (B) and medial (C) aspects of the osteotomy site. The vertical white lines on the dorsal plane proton density weighted images (D-F) correspond with the sagittal plane slices for the lateral, middle and medial aspects of the tibial osteotomy respectively.

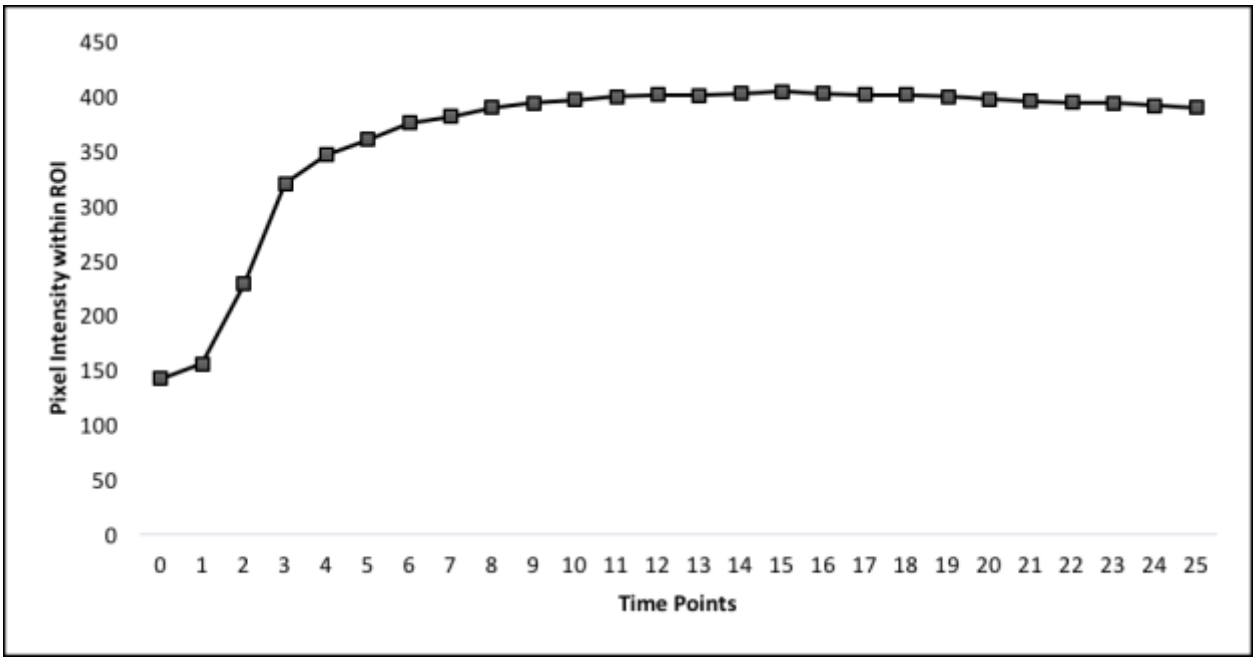

Figure 3.2. Graphical representation of dynamic contrast enhanced (DCE) MRI signal intensity over time. There was an initial steep increase in pixel intensity, followed by a plateau without evidence of signal washout. This trend existed for all patients included in the study.

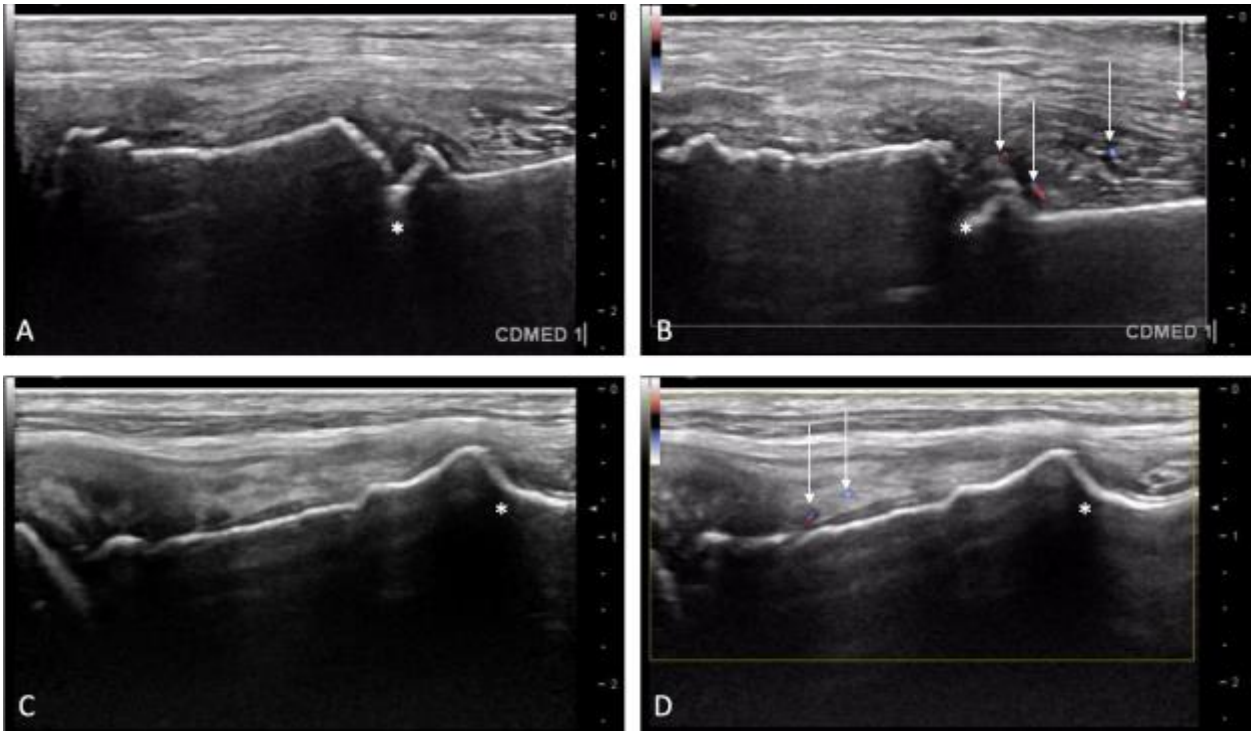

Figure 3.3. Representative images from the ultrasonographic exams of one patient over time. At 4w post-operatively, the osteotomy site (asterisk) is conspicuous, with irregular margins and lack of bridging cortices appreciated on B-mode ultrasonography (A). There are multiple power Doppler signals present (arrows) in the soft tissues surrounding the osteotomy (B). By 10w post-operatively, B-mode ultrasonography (C) reveals smooth and confluent cortical margins, with a general decrease in the number and size of vessels identified (arrows) on power Doppler (D).

REFERENCES

1. Wilke VL, Robinson DA, Evans RB, Rothschild MF, Conzemius MG. Estimate of the annual economic impact of treatment of cranial cruciate ligament injury in dogs in the United States. *Journal of the American Veterinary Medical Association*. 2005;227:1604-1607.

2. Henry GA. Fracture Healing and Complications. In: THRALL DE, ed. *Textbook of Veterinary Diagnostic Radiology*. 6 ed. St. Louis: Elsevier Saunders; 2013:283-306.

3. Bolog N, Nanz D, Weishaupt D. Muskuloskeletal MR imaging at 3.0 T: current status and future perspectives. *Eur Radiol*. 2006;16(6):1298-1307. doi:10.1007/s00330-006-0184-7.

4. D'ANJOU M-A. Principles of Computed Tomography and Magnetic Resonance Imaging. In: THRALL DE, ed. *Textbook of Veterinary Diagnostic Radiology*. 6 ed. Magnetic Resonance Imaging. St. Louis: Elsevier Saunders; 2013:61-73.

5. Bushong SC. An Overview of Magnetic Resonance Imaging. In: *Magnetic Resonance Imaging*. 3rd ed. St. Louis; 2003:3-17.

6. Westbrook C. *MRI at a Glance*. Malden: Blackwell Science Ltd; 2002.

7. Plewes DB, Kucharczyk W. Physics of MRI: A primer. *J Magn Reson Imaging*. 2012;35(5):1038-1054. doi:10.1002/jmri.23642.

8. Bushberg JT, Seibert JA, Leidholdt EM, Boone JM. *The Essential Physics of Medical Imaging*. 2nd ed. Philadelphia: Lippincott Williams & Wilkins; :373-380.

9. Gavin PR, Bagley RS. Ames: Wiley-Blackwell; 2009:2-7.

10. Plewes DB, Kucharczyk W. Physics of MRI: A primer. *J Magn Reson Imaging*. 2012;35(5):1038-1054. doi:10.1002/jmri.23642.

11. Bushong SC. Nuclear Magnetism. In: *Magnetic Resonance Imaging*. 3rd ed. St. Louis: Mosby; 2003:41-50.

12. Bushong SC. Equilibrium-Saturation. In: *Magnetic Resonance Imaging*. 3rd ed. St. Louis: Mosby; 2003:51-58.

13. Bushberg JT, Seibert JA, Leidholdt EM, Boone JM. Magnetic Resonance Basics. In: *The Essential Physics of Medical Imaging*. 3rd ed. Return to Equilibrium: T1 Relaxation. Philadelphia: Lippincott Williams & Wilkins; 2012:417-419.

14. Bushong SC. The Musical Score. In: *Magnetic Resonance Imaging*. 3rd ed. St. Louis: Mosby; 2003:205-224.

15. Bushong SC. Chemical Shift and Magnetization Transfer. In: *Magnetic Resonance Imaging*. 3rd ed. St. Louis: Mosby; 2003:278-286.

16. Dillenseger JP, Molière S, Choquet P, Goetz C, Ehlinger M, Bierry G. An illustrative review to understand and manage metal-induced artifacts in musculoskeletal MRI: a primer and updates. *Skeletal Radiology*. 2016;45(5):677-688. doi:10.1007/s00256-016-2338-2.

17. Bushong SC. Magnetic Resonance Artifacts. In: *Magnetic Resonance Imaging*. 3rd ed. St. Louis: Mosby; 2003:374-392.

18. Ipek Ö. Radio-frequency coils for ultra-high field magnetic resonance. *Analytical Biochemistry*. April 2017:1-7. doi:10.1016/j.ab.2017.03.022.

19. Notohamiprodjo M, Horng A, Kuschel B, et al. 3D-imaging of the knee with an optimized 3D-FSE-sequence and a 15-channel knee-coil. *European Journal of Radiology*. 2012;81(11):3441-3449. doi:10.1016/j.ejrad.2012.04.020.

20. Bushberg JT, Seibert JA, Leidholdt EM, Boone JM. Basic Pulse Sequences. In: *The Essential Physics of Medical Imaging*. 3rd ed. Philadelphia: Lippincott Williams & Wilkins; 2012:421-438.

21. Gavin PR. Basic Physics. In: Ames; 2009:4-7.

22. BAKER MA, MACDONALD I. EVALUATION OF MAGNETIC RESONANCE SAFETY OF VETERINARY RADIOFREQUENCY IDENTIFICATION DEVICES AT 1 T. *Veterinary Radiology & Ultrasound*. 2010;52(2):161-167.

23. David FH, Grierson J, Lamb CR. EFFECTS OF SURGICAL IMPLANTS ON HIGH-FIELD MAGNETIC RESONANCE IMAGES OF THE NORMAL CANINE STIFLE. *Veterinary Radiology & Ultrasound*. 2012;16(Suppl):n/a–n/a. doi:10.1111/j.1740-8261.2011.01901.x.

24. Lee M-J, Kim S, Lee S-A, et al. Overcoming Artifacts from Metallic Orthopedic Implants at High-Field-Strength MR Imaging and Multi-detector CT. *RadioGraphics*. 2007;27(3):791-803. doi:10.1148/rg.273065087.

25. Hargreaves BA, Worters PW, Pauly KB, Pauly JM, Koch KM, Gold GE. Metal-Induced Artifacts in MRI. *American Journal of Roentgenology*. 2011;197(3):547-555. doi:10.2214/AJR.11.7364.

26. Bachschmidt TJ, Sutter R, Jakob PM, Pfirrmann CWA, Nittka M. Knee implant imaging at 3 Tesla using high-bandwidth radiofrequency pulses. *J Magn Reson Imaging*. 2014;41(6):1570-1580. doi:10.1002/jmri.24729.

27. Hecht S, ADAMS WH, NARAK J, THOMAS WB. MAGNETIC RESONANCE IMAGING SUSCEPTIBILITY ARTIFACTS DUE TO METALLIC FOREIGN BODIES. *Veterinary Radiology & Ultrasound*. 2011;52(4):409-414.

28. Saito M, Ono S, Kayanuma H, Honnami M, Muto M, Une Y. Evaluation of the Susceptibility Artifacts and TIssue Injury Caused by Implanted Microchips in Dogs on

1.5T Magnetic Resonance Imaging. *Journal of Veterinary Medicine and Science*. June 2000:1-7.

29. Suh J-S, Jeong E-K, Shin K-H, et al. Minimizing artifacts caused by metallic implants at MR imaging: experimental and clinical studies. *American Journal of Roentgenology*. 2016;171:1207-1213.

30. Hecht S, ADAMS WH, NARAK J, THOMAS WB. MAGNETIC RESONANCE IMAGING SUSCEPTIBILITY ARTIFACTS DUE TO METALLIC FOREIGN BODIES. *Veterinary Radiology & Ultrasound*. 2011;52(4):409-414. doi:10.1111/j.1740-8261.2011.01809.x.

31. Choi S-J, Koch KM, Hargreaves BA, Stevens KJ, Gold GE. Metal Artifact Reduction With MAVRIC SL at 3-T MRI in Patients With Hip Arthroplasty. *American Journal of Roentgenology*. 2015;204(1):140-147. doi:10.2214/AJR.13.11785.

32. Jungmann PM, Ganter C, Schaeffeler CJ, et al. View-Angle Tilting and Slice-Encoding Metal Artifact Correction for Artifact Reduction in MRI: Experimental Sequence Optimization for Orthopaedic Tumor Endoprostheses and Clinical Application. Zhang H, ed. *PLoS ONE*. 2015;10(4):e0124922–18. doi:10.1371/journal.pone.0124922.

33. Simpler RE, Kerwin SC, Eichelberger BM, et al. EVALUATION OF THE WARP-TURBO SPIN ECHO SEQUENCE FOR 3 TESLA MAGNETIC RESONANCE IMAGING OF STIFLE JOINTS IN DOGS WITH STAINLESS STEEL TIBIAL PLATEAU LEVELING OSTEOTOMY IMPLANTS. *Veterinary Radiology & Ultrasound*. 2014;55(4):414-419. doi:10.1111/vru.12141.

34. van Bree H, Dingemanse W, Gielen I. MRI and arthroscopy for evaluation of shoulder joint pathology. *ECVS Proceedings*. June 2011:1-3.

35. Biggi M, Zani DD, De Zani D, Di Giancamillo M. Magnetic resonance imaging findings of bone marrow lesions in the equine distal tarsus. *Equine Vet Educ*. 2011;24(5):236-241. doi:10.1111/j.2042-3292.2011.00288.x.

36. Baron K, Neumayer B, Widek T, et al. Quantitative MR imaging in fracture dating—Initial results. *Forensic Science International*. 2016;261:61-69. doi:10.1016/j.forsciint.2016.01.020.

37. Buckley R. *AO Principles of Fracture Management*. Vol 1. (Ruedi TP, Ruedi R, eds.). 2007.

38. de Kerviler E, Leroy-Willig A, Clement O, Frija J. Fat suppresion techniques in MRI: an update. *Biomed Pharmacother*. 1998;52:69-75.

39. Del Grande F, Santini F, Herzka DA, et al. Fat-Suppression Techniques for 3-T MR Imaging of the Musculoskeletal System. *RadioGraphics*. 2014;34(1):217-233. doi:10.1148/rg.341135130.

40. Sonoda K, Yamamoto T, Motomura G, Karasuyama K, Kubo Y, Iwamoto Y. Fat-suppressed T2-weighted MRI appearance of subchondral insufficiency fracture of the femoral head. *Skeletal Radiology*. September 2016:1-7. doi:10.1007/s00256-016-2462-z.

41. Del Grande F, Santini F, Herzka DA, et al. Fat-Suppression Techniques for 3-T MR Imaging of the Musculoskeletal System. *RadioGraphics*. 2014;34(1):217-233. doi:10.1148/rg.341135130.

42. Kirchgesner T, Perlepe V, Michoux N, Larbi A, Berg BV. Fat suppression at 2D MR imaging of the hands: Dixon method versus CHESS technique and STIR sequence. *European Journal of Radiology*. 2017;89:40-46. doi:10.1016/j.ejrad.2017.01.011.

43. Lewis M, Ebreo D, Malcolm PN, et al. Pharmacokinetic modeling of multislice dynamic contrast-enhanced MRI in normal-healing radial fractures: A pilot study. *J Magn Reson Imaging*. 2015;43(3):611-619. doi:10.1002/jmri.25039.

44. Fischer C, Nissen M, Schmidmaier G, Bruckner T, Kauczor H-U, Weber M-A. Dynamic contrast-enhanced magnetic resonance imaging (DCE-MRI) for the prediction of non-union consolidation. *Injury*. January 2017:1-7. doi:10.1016/j.injury.2017.01.021.

45. Massie AM, Kapatkin AS, Fuller MC, Verstraete FJM, Arzi B. Outcome of nonunion fractures in dogs treated with fixation, compression resistant matrix, and recombinant human bone morphogenetic protein-2. *Veterinary and Comparative Orthopaedics and Traumatology*. 2017;30(2):153-159. doi:10.3415/VCOT-16-05-0082.

46. Ehrhart N, Kraft S, Conover D, Rosier RN, Schwarz EM. Quantification of Massive Allograft Healing with Dynamic Contrast Enhanced-MRI and Cone Beam-CT: A Pilot Study. *Clin Orthop Relat Res*. 2008;466(8):1897-1904. doi:10.1007/s11999-008-0293-5.

47. Chen W-T, Shih TT-F, Chen R-C, et al. Blood perfusion of vertebral lesions evaluated with gadolinium-enhanced dynamic MRI: In comparison with compression fracture and metastasis. *J Magn Reson Imaging*. 2002;15(3):308-314. doi:10.1002/jmri.10063.

48. Konishiike T, Makihata E, Tago H, Sato T, Inoue H. Acute fracture of the neck of the femur: an assessment of perfusion of the head by dynamic MRI. *J Bone Joint Surg*. 1999;81(B):596-599.

49. Schoierer O, Bloess K, Bender D, et al. Dynamic contrast-enhanced magnetic resonance imaging can assess vascularity within fracture non-unions and predicts good outcome. *Eur Radiol*. 2013;24(2):449-459. doi:10.1007/s00330-013-3043-3.

50. MD AB, MD DT, MD JCW. Nonunion of the Femur and Tibia: an Update. *Orthopedic Clinics of NA*. 2016;47(2):365-375. doi:10.1016/j.ocl.2015.09.010.

51. MD MRB, PhD DPO. Management of Aseptic Tibial and Femoral Diaphyseal Nonunions Without Bony Defects. *Orthopedic Clinics of NA*. 2016;47(1):67-75. doi:10.1016/j.ocl.2015.08.009.

52. Malhotra A, Pelletier MH, Yu Y, Walsh WR. Can platelet-rich plasma (PRP) improve bone healing? A comparison between the theory and experimental outcomes. *Arch Orthop Trauma Surg*. 2012;133(2):153-165. doi:10.1007/s00402-012-1641-1.

53. Intini G. The use of platelet-rich plasma in bone reconstruction therapy. *Biomaterials*. 2009;30(28):4956-4966. doi:10.1016/j.biomaterials.2009.05.055.

54. Iqbal J, Pepkowitz SH, Klapper E. Platelet-Rich Plasma for the Replenishment of Bone. *Curr Osteoporos Rep*. 2011;9(4):258-263. doi:10.1007/s11914-011-0080-1.

55. Roffi A, Di Matteo B, Krishnakumar GS, Kon E, Filardo G. Platelet-rich plasma for the treatment of bone defects: from pre-clinical rational to evidence in the clinical practice. A systematic review. *International Orthopaedics*. January 2017:1-17. doi:10.1007/s00264-016-3342-9.

56. Gianakos A, Zambrana L, Savage-Elliott I, Lane JM, Kennedy JG. Platelet-Rich Plasma in the Animal Long-Bone Model: An Analysis of Basic Science Evidence. *Orthopedics*. 2015;38(12):e1079-e1090. doi:10.3928/01477447-20151120-04.

57. Duerr FM, Martin KW, Rishniw M, Palmer RH, Selmic LE. Treatment of canine cranial cruciate ligament disease. *Veterinary and Comparative Orthopaedics and Traumatology*. 2014;27(6):478-483. doi:10.3415/VCOT-14-03-0047.

58. Kim SE, LEWIS DD, Pozzi A. Effect of Tibial Plateau Leveling Osteotomy on Femorotibial Subluxation: In Vivo Analysis during Standing. *Veterinary Surgery*. 2012;41(4):465-470. doi:10.1111/j.1532-950X.2012.00973.x.

59. Fitzpatrick N, Solano MA. Predictive Variables for Complications after TPLO with Stifle Inspection by Arthrotomy in 1000 Consecutive Dogs. *Veterinary Surgery*. 2010;39(4):460-474. doi:10.1111/j.1532-950X.2010.00663.x.

60. Bergh MS, Peirone B. Complications of tibial plateau levelling osteotomy in dogs. *Veterinary and Comparative Orthopaedics and Traumatology*. 2012;25(5):349-358. doi:10.3415/VCOT-11-09-0122.

61. Franklin SP, Garner BC, Cook JL. Characteristics of canine platelet-rich plasma prepared with five commercially available systems. *American Journal of Veterinary Research*. 2015;76:822-827.

62. Visser LC, Arnoczky SP, Caballero O, Egerbacher M. Platelet-Rich Fibrin Constructs Elute Higher Concentrations of Transforming Growth Factor-β1 and Increase Tendon Cell Proliferation Over Time when Compared to Blood Clots: A Comparative In Vitro Analysis. *Veterinary Surgery*. 2010;39(7):811-817. doi:10.1111/j.1532-950X.2010.00739.x.

63. Barry S. Non-steroidal anti-inflammatory drugs inhibit bone healing: A review. *Veterinary and Comparative Orthopaedics and Traumatology*. 2010;23(6):385-392. doi:10.3415/VCOT-10-01-0017.

64. Kieves NR, MacKay CS, Adducci K, et al. High energy focused shock wave therapy accelerates bone healing. *Veterinary and Comparative Orthopaedics and Traumatology*. 2015;28(6):425-432. doi:10.3415/VCOT-15-05-0084.

65. Conkling AL, Fagin B, Daye RM. Comparison of Tibial Plateau Angle Changes after Tibial Plateau Leveling Osteotomy Fixation with Conventional or Locking Screw Technology. *Veterinary Surgery*. 2010;39(4):475-481. doi:10.1111/j.1532-950X.2010.00656.x.

66. RISSELADA M, KRAMER M, de Rooster H, Taeymans O, VERLEYEN P, van BREE H. Ultrasonographic and Radiographic Assessment of Uncomplicated Secondary Fracture Healing of Long Bones in Dogs and Cats. *Veterinary Surgery*. 2005;34(2):99-107. doi:10.1111/j.1532-950X.2005.00017.x.

67. RISSELADA M, KRAMER M, van Bree H. APPROACHES FOR ULTRASONOGRAPHIC EVALUATION OF LONG BONES IN THE DOG. *Veterinary Radiology & Ultrasound*. 2003;44(2):214-220.

68. RISSELADA M, van Bree H, KRAMER M, Duchateau L, VERLEYEN P, SAUNDERS JH. ULTRASONOGRAPHIC ASSESSMENT OF FRACTURE HEALING AFTER PLATE OSTEOSYNTHESIS. *Veterinary Radiology & Ultrasound*. 2007;48(4):368-372. doi:10.1111/j.1740-8261.2007.00258.x.

69. RISSELADA M, KRAMER M, Saunders JH, VERLEYEN P, van BREE H. POWER DOPPLER ASSESSMENT OF THE NEOVASCULARIZATION DURING UNCOMPLICATED FRACTURE HEALING OF LONG BONES IN DOGS AND CATS. *Veterinary Radiology & Ultrasound*. 2006;47(3):301-306. doi:10.1111/j.1740-8261.2006.00144.x.

70. Cook JL, Evans R, Conzemius MG, et al. Proposed Definitions and Criteria for Reporting Time Frame, Outcome, and Complications For Clinical Orthopedic Studies in Veterinary Medicine. *Veterinary Surgery*. 2010;39(8):905-908. doi:10.1111/j.1532-950X.2010.00763.x.

71. Gauthier O, Rabillard M, Grand JG, Dalibert E, Fellah B, Niebauer GW. Effects of autologous platelet rich plasma gel and calcium phosphate biomaterials on bone healing in an ulnar ostectomy model in dogs. *Veterinary and Comparative Orthopaedics and Traumatology*. 2009:1-7. doi:10.3415/VCOT-09-04-0048.

72. Souza TFB, Andrade AL, Ferrreira GTNM, et al. Healing and expression of growth factors (TGF-β and PDGF) in canine radial ostectomy gap containing platelet-rich plasma. *Veterinary and Comparative Orthopaedics and Traumatology*. 2012;25(6):445-452. doi:10.3415/VCOT-10-10-0146.

73. Rodriguez IA, Growney Kalaf EA, Bowlin GL, Sell SA. Platelet-Rich Plasma in Bone Regeneration: Engineering the Delivery for Improved Clinical Efficacy. *BioMed Research International*. 2014;2014(3):1-15. doi:10.1155/2014/392398.

74. Maeno S, Niki Y, Matsumoto H, et al. The effect of calcium ion concentration on osteoblast viability, proliferation and differentiation in monolayer and 3D culture. *Biomaterials*. 2005;26(23):4847-4855. doi:10.1016/j.biomaterials.2005.01.006.

75. Sadeghi-Ataabadi M, Mostafavi-pour Z, Vojdani Z, Sani M, Latifi M, Talaei-Khozani T. Fabrication and characterization of platelet-rich plasma scaffolds for tissue engineering applications. *Materials Science & Engineering C*. 2017;71(C):372-380. doi:10.1016/j.msec.2016.10.001.

76. Diesen DL, Lawson JH. Bovine Thrombin: History, Use, and Risk in the Surgical Patient. *Vascular*. 2008;16(1):529-536.

77. Boswell SG, Schnabel LV, Mohammed HO, Sundman EA, Minas T, Fortier LA. Increasing Platelet Concentrations in Leukocyte-Reduced Platelet-Rich Plasma Decrease Collagen Gene Synthesis in Tendons. *The American Journal of Sports Medicine*. 2014;42(1):42-49. doi:10.1177/0363546513507566.

78. Hatakeyama I, Marukawa E, Takahashi Y, Omura K. Effects of Platelet-Poor Plasma, Platelet-Rich Plasma, and Platelet-Rich Fibrin on Healing of Extraction Sockets with Buccal Dehiscence in Dogs. *Tissue Engineering Part A*. November 2013:131127122606000-131127122606009. doi:10.1089/ten.tea.2013.0058.

79. Warzee CC, Dejardin LICM, Arnoczky SP, Perry RL. Effect of tibial plateau leveling on cranial and caudal tibial thrusts in canine cranial cruciate-deficient stifles: An in vitro experimental study. *Veterinary Surgery*. 2001;30(3):278-286. doi:10.1053/jvet.2001.21400.

80. Reif U, Hulse DA, HAUPTMAN JG. Effect of tibial plateau leveling on stability of the canine cranial cruciate[ndash]deficient stifle joint: An in vitro study. *Veterinary Surgery*. 2002;31(2):147-154. doi:10.1053/jvet.2002.31041.

81. Sande R. Radiography of Orthopedic Trauma and Fracture Repair. *Veterinary Clinics of NA: Small Animal Practice*. 1999;29(5):1247-1260.

82. Ricciardi L, Perissinotto A, Dabala M. External callus development on ultrasound and its mechanical correlation. *Ital J Orthop Traumatol*. 1992;18(2):223-229.

83. Remedios A. Bone and Bone Healing. *Veterinary Clinics of NA: Small Animal Practice*. 1999;29(5):1029-1044.

84. D'ANJOU M-A, Penninck D. Practical Physical Concepts and Artifacts. In: *Atlas of Small Animal Ultrasonography*. 2nd ed. Ames; 2015:1-18.

85. D'ANJOU M-A, MOREAU M, TRONCY É, et al. Osteophytosis, Subchondral Bone Sclerosis, Joint Effusion and Soft Tissue Thickening in Canine Experimental Stifle Osteoarthritis: Comparison Between 1.5 T Magnetic Resonance Imaging and Computed Radiography. *Veterinary Surgery*. 2008;37(2):166-177. doi:10.1111/j.1532-950X.2007.00363.x.

86. Kanamura H, Arai Y, Hara K, et al. Quantitative evaluation of revascularization at bone tunnels and grafts with contrast-enhanced magnetic resonance angiography after anterior cruciate ligament reconstruction. *International Orthopaedics*. 2016;40:1531-1536. doi:10.1007/s00264-015-3092-0.

87. Taylor-Brown F, Lamb CR, Tivers MS, Li A. Magnetic resonance imaging for detection of late meniscal tears in dogs following tibial tuberosity advancement for treatment of cranial cruciate ligament injury. *Veterinary and Comparative Orthopaedics and Traumatology*. 2014;27(2):141-146. doi:10.3415/VCOT-13-08-0107.

88. Baron K, Neumayer B, Amerstorfer E, et al. Time-Dependent Changes in T1 during Fracture Healing in Juvenile Rats: A Quantitative MR Approach. Wallace JM, ed. *PLoS ONE*. 2016;11(11):e0164284–14. doi:10.1371/journal.pone.0164284.

89. Rupreht M, Jevtič V, Serša I, Vogrin M, Šeruga T, Jevšek M. Quantitative evaluation of the tibial tunnel after anterior cruciate ligament reconstruction using diffusion weighted and dynamic contrast enhanced MRI: a follow-up feasibility study. *Skeletal Radiology*. 2011;41(5):569-574. doi:10.1007/s00256-011-1256-6.

90. Hargreaves BA, Worters PW, Pauly KB, Pauly JM, Koch KM, Gold GE. Metal-Induced Artifacts in MRI. *American Journal of Roentgenology*. 2011;197(3):547-555. doi:10.2214/AJR.11.7364.